

Surface Cyclones in the ERA-40 Dataset (1958–2001). Part I: Novel Identification Method and Global Climatology

HEINI WERNLI

Institute for Atmospheric and Climate Science, ETH Zürich, Zurich, Switzerland, and Institute for Atmospheric Physics, University of Mainz, Mainz, Germany

CORNELIA SCHWIERZ

Institute for Atmospheric and Climate Science, ETH Zürich, Zurich, Switzerland

(Manuscript received 5 January 2005, in final form 1 February 2006)

ABSTRACT

A novel method is introduced to generate climatological frequency distributions of meteorological features from gridded datasets. The method is used here to derive a climatology of extratropical cyclones from sea level pressure (SLP) fields. A simple and classical conception of cyclones is adopted where a cyclone is identified as the finite area that surrounds a local SLP minimum and is enclosed by the outermost closed SLP contour. This cyclone identification procedure can be applied to individual time instants, and climatologies of cyclone frequency, f_c , are obtained by simple time averaging. Therefore, unlike most other climatologies, the method is not based on the application of a tracking algorithm and considers the size of cyclones. In combination with a conventional cyclone center tracking algorithm that allows the determination of cyclone life times and the location of cyclogenesis and cyclolysis, additional frequency fields can be obtained for special categories of cyclones that are generated in, move through, or decay in a specified geographical area.

The method is applied to the global SLP dataset for the time period 1958–2001 from the latest 40-yr European Centre for Medium-Range Weather Forecasts (ECMWF) Re-Analysis (ERA-40). In the Northern Hemisphere and during winter, the cyclone frequency field has three maxima in the Pacific storm track (with f_c up to 35%), the Atlantic storm track (with f_c up to 32%), and the Mediterranean (with f_c up to 15%). During the other seasons the f_c values are generally reduced in midlatitudes and the subtropical monsoon areas appear as regions with enhanced f_c . In the Southern Hemisphere, the seasonal variations are smaller with year-round maxima of f_c in the belt from 50° to 70°S (along the coast of Antarctica, with maximum values of almost 40%) and to the east of the Andes (with f_c up to 35% during summer). Application of a lifetime threshold value significantly reduces f_c , in particular over and close to the continents. Subsets of cyclone frequency fields are calculated for several subjectively chosen regions of cyclone genesis, passage, and lysis. They show some interesting aspects of the behavior of extratropical cyclones; cyclones that decay along the U.S. West Coast, for instance, have a short lifetime and originate almost exclusively from the eastern North Pacific, whereas long-lived and long-distance Pacific cyclones terminate farther north in the Gulf of Alaska.

The approach to calculate frequency distributions of atmospheric flow structures as introduced in this study can be easily applied to gridded data from global atmospheric models and assimilation systems. It combines the counts of atmospheric features with their area of influence, and hence provides a robust and easily interpretable measure of key meteorological structures when comparing and evaluating different analysis datasets and climate model integrations. Further work is required to comprehensively exploit the presented global ERA-40 cyclone climatology, in particular, aspects of its interannual variability.

1. Introduction

Cyclones and anticyclones are the dominant synoptic-scale features on midlatitude surface weather charts.

Corresponding author address: Heini Wernli, Institute for Atmospheric Physics, University of Mainz, Becherweg 21, D-55099 Mainz, Germany.
E-mail: wernli@uni-mainz.de

The former are typically accompanied by mesoscale frontal structures, damaging winds, and heavy precipitation; the latter are frequently associated with calm weather and, for instance over Europe, sometimes with extreme temperatures (cold in winter and hot in summer). Knowledge of the geographical distribution of the origin, growth, translation, and finally decay of these systems is of central importance to characterize

extratropical climate. Köppen (1881) performed a first climatology of depressions from an analysis of sea level pressure (SLP) charts and noticed the occurrence of preferred cyclone tracks in the North Atlantic region. Since then, many techniques have been developed and applied (manually and automatically) to different datasets to gain insight into the present-day climatological distribution of surface (anti)cyclones. Clearly, the issues of climate variability and trends and the availability of quasi-consistent reanalysis datasets have increased the interest in reliable cyclone (and anticyclone) climatologies and identification procedures that can be used also to analyze trends in the observations over recent decades (e.g., Simmonds and Keay 2000a; McCabe et al. 2001) and to investigate climate change simulations from a synoptic perspective (e.g., Hall et al. 1994; Sinclair and Watterson 1999; Fyfe 2003; Raible and Blender 2004).

There are different approaches to define meaningful indices of cyclone activity and to compile climatologies. Recent studies highlight the fact that no single activity index captures all the relevant information about cyclone intensity, scale, and propagation. Therefore, they present either a combination of indices (Paciorek et al. 2002) or develop new integrated activity measures (Zhang et al. 2004). Most of the existing cyclone climatologies use algorithms that can be categorized into nontracking and tracking techniques. The former regard cyclones as point objects represented by their center (e.g., the location of the SLP minimum) and yield climatological cyclone center density fields (e.g., Lambert 1988; Zhang et al. 2004). This approach is straightforward but cannot provide information about the genesis and lysis of cyclones. Most existing climatologies belong to the second category and are based on some kind of cyclone tracking technique. They also represent cyclones by their center and compute cyclone tracks as meteorologically meaningful connections of cyclone positions in time. The track's initial point is then regarded as the location of cyclogenesis, and its final point as the location of cyclolysis.

However, it should be noted that the identification of cyclone centers, the tracking, and the computation of track densities, are technically far from straightforward and unavoidably associated with uncertainties. Some comments on this issue and other important aspects of cyclone climatologies follow in the next paragraphs. More comprehensive introductions to the topic of cyclone identification and tracking can be found, for instance, in the recent publications by Sickmüller et al. (2000), Zolina and Gulev (2002), and Hanson et al. (2004).

Algorithms used to compile cyclone climatologies re-

quire a suitable choice of parameters that are used to (i) identify cyclones, (ii) determine a likely continuation of a cyclone track, and (iii) retaining "meaningful tracks" (e.g., by choosing a minimum track length and/or a minimum cyclone lifetime). The parameters, in particular those used in step (iii), are not determined purely on a physical basis and are therefore somehow arbitrary. For instance, Sickmüller et al. (2000) only consider cyclones with a lifetime of at least 3 days, whereas this threshold is set to 2 days in the studies of Sinclair (1995) and Hoskins and Hodges (2002, hereafter HH02), and to 1 day in the studies of Simmonds and Keay (2000b) and Hanson et al. (2004). The choice of this parameter strongly influences the size of the climatological ensemble of cyclone tracks because most of the cyclones have short lifetimes of less than 2 days (e.g., Nielsen and Dole 1992; Trigo et al. 1999; Hanson et al. 2004). Some studies (e.g., Sinclair 1995; Blender et al. 1997) introduce an additional parameter to distinguish between stationary and moving cyclones. The actual tracking [step (ii)] is particularly susceptible to the temporal and spatial resolution. With a poor temporal resolution the evolution of the systems cannot be captured in detail (Blender and Schubert 2000; Zolina and Gulev 2002), whereas with a very high spatial resolution many small-scale and short-lived systems are resolved that render the correct identification of the track extension difficult (as will be shown in a few examples in section 2c). Also for step (i), there are several possibilities to identify a cyclone center. The simplest criterion requires the SLP grid point value to be smaller than at the four or eight neighboring grid points. Depending on the considered variable (SLP, geopotential height, or relative vorticity) it matters whether local extrema are identified from the full field or from a suitable "anomaly field." For instance HH02 subtract the large-scale components of the fields in order to better capture the synoptic systems. Various possibilities for how this can be done are discussed in Anderson et al. (2003).

Note also that the Eulerian, so-called dynamic, storm-track measures, like the high-frequency geopotential height variance or eddy kinetic energy (Blackmon et al. 1977), are to a certain degree subjective, such as in the choice of the filtering interval for the high- or bandpass filters. For instance, the application of high-frequency filters favors fast moving transient features above possibly more rapidly growing but slower moving cyclones.

In this study a novel method is introduced to automatically identify low pressure systems [the above step (i)] and their spatial extension from gridded SLP fields (section 2). The method allows one to determine cyclone frequency fields that differ from the previously

investigating cyclone counts and track densities. These climatological results will be shown in section 3 for the 40-Yr European Centre for Medium-Range Weather Forecasts (ECMWF) Re-Analysis (ERA-40) dataset. In combination with a conventional tracking algorithm, the approach can also serve to determine the locations of genesis and lysis (section 4) and to compute subsets of the total cyclone frequency field for selected classes of extratropical low pressure systems (section 5). Section 6 contains a discussion of the caveats of the method and compares the results qualitatively with previous cyclone climatologies. The final section summarizes the study and provides a brief outlook on further possibilities and applications.

2. The methodology

This section introduces a method for obtaining climatological frequency fields of surface cyclones that combines the counts of cyclones with their area of influence. Examples are presented to illustrate the method, and a conventional tracking algorithm is briefly explained that will be used to obtain further information about the cyclone life cycles.

The data used in this study are the global SLP fields from the ERA-40 dataset, available every 6 h. ERA-40 data have a spectral resolution of T159 and have been interpolated for the present analysis on a longitude–latitude grid with 1° horizontal resolution. For completeness it is mentioned that the examples shown in this methodological section are based on the earlier ERA-15 dataset with a slightly coarser spectral resolution of T106 interpolated on a $1.125^\circ \times 1.125^\circ$ grid.¹ Basic information about the ERA-40 project can be found in Simmons and Gibson (2000). It is important to note that ERA-40 data have been produced with a frozen three-dimensional variational data assimilation system, but because of significant changes in the atmospheric observing system since the late 1950s the resulting dataset cannot be fully consistent. In particular, the advent of satellite observations in 1979 greatly impacts on the resulting analyses in regions that are not well covered by conventional observing systems such as the SH. Bengtsson et al. (2004) discussed this issue and showed that in the SH the analyzed SLP field is dominated by the satellite observations and that therefore

¹ Earlier studies (e.g. Sinclair 1997) indicated that a latitude–longitude projection may not be ideal near the pole for cyclone climatologies based upon the vorticity field. For the smoother SLP fields used in this study we do not expect that this problem significantly affects our results, however a thorough test is left for future investigation.

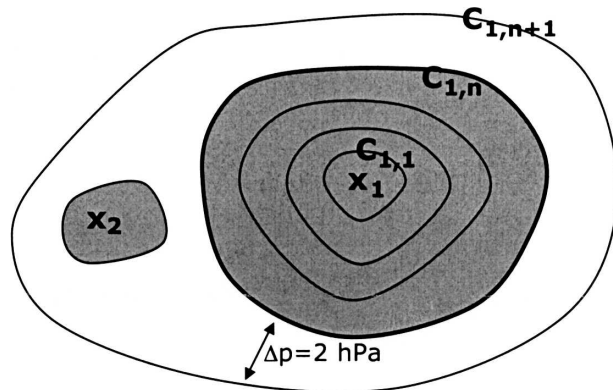


FIG. 1. Schematic illustration for the cyclone identification procedure (see text for details).

the SLP dataset from 1958 to 2001 cannot be regarded as perfectly consistent. In the present study, this aspect is not addressed and climatologies will be shown for the entire time period without distinguishing the subperiods before and after satellite data have become available.

a. The identification of low pressure systems

The procedure to identify all cyclones from a SLP field p at a certain time instant consists of three steps, of which the second one is nonstandard and explained in more detail below:

- (i) First, cyclone centers are determined as local minima in the array of SLP grid point values. A grid point is considered a cyclone center if its SLP value is smaller than the value at each of its eight neighboring grid points. This is a weak condition compared to the criteria applied in some earlier studies and leads to a large number of identified cyclones. As summarized by Haak and Ulbrich (1996), the number of cyclones is often reduced with additional criteria. For instance, the difference between the SLP minimum and its neighboring values has to be larger than a certain threshold, and/or the curvature of the SLP field at the local minimum must exceed a specific value.
- (ii) In a second step, for every local SLP minimum the outermost closed SLP contour is determined that encloses only the SLP minimum under consideration (see Fig. 1). The area enclosed by this outermost closed contour is regarded as the cyclone and a “cyclone field” c is defined with values $c = 1$ at grid points inside the identified cyclone and $c = 0$ outside this area. This cyclone definition agrees with one of the possibilities mentioned, but not further pursued, by Nielsen and Dole (1992). Also, Robertson and Smith (1980) used a similar

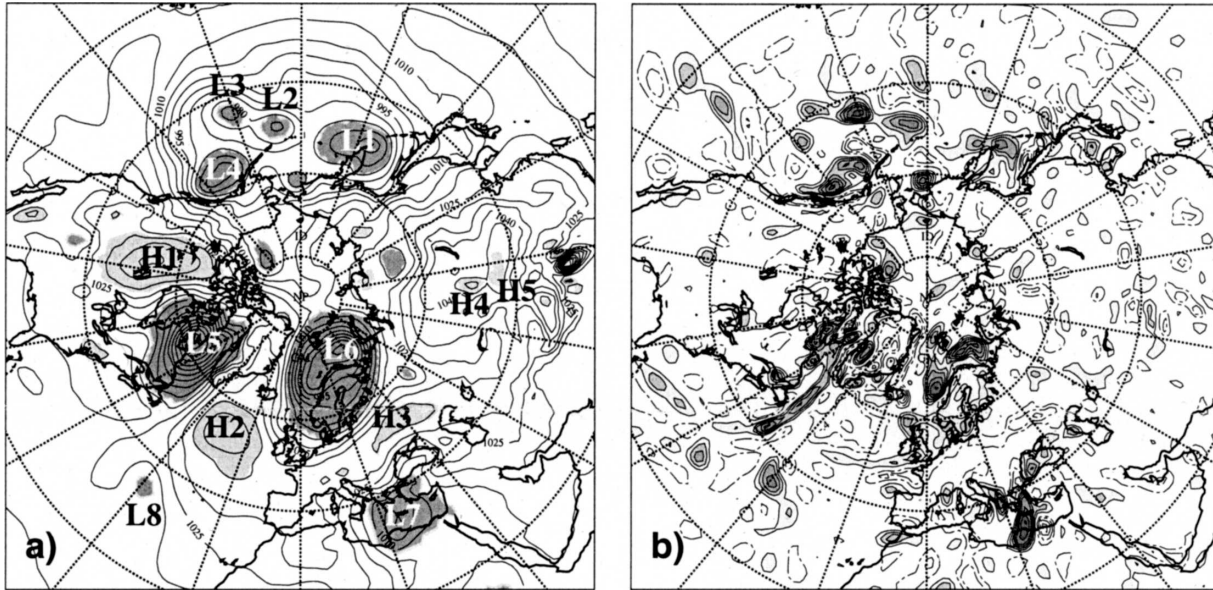


FIG. 2. (a) Illustrative example for the performance of the (anti)cyclone identification algorithm at 1200 UTC 9 Jan 1981. Shown are the SLP field (contour interval = 5 hPa) and the identified cyclones (i.e., regions where the cyclone field $c = 1$, dark shading) and anticyclones (regions where the anticyclone field is equal to 1, light shading). (b) The 1000-hPa relative vorticity field at the same time as (a). Gray shading is used for positive and dashed-dotted lines for negative values (contour interval = $0.2f$); zero line is omitted.

definition to demark the vicinity of cyclones for energy budget calculations, and Sinclair (1997) followed a related approach to calculate the cyclones' circulation as a measure of their intensity.

- (iii) Finally, in addition to the cyclone field c some characteristics are archived for every individual cyclone, such as the geographical location of the cyclone center, the size of the cyclone, the central SLP value and the SLP value of the outermost closed contour. This information is required for the subsequent tracking algorithm and for further statistical evaluations of cyclone characteristics.

For step (i), an algorithm has been developed, which, for every local SLP minimum, searches a set of still larger enclosing contours at a pressure interval Δp until the contour encloses one of the other local minima identified in step (i). The second last contour (which does not enclose a second minimum) is taken as the outermost closed contour. Figure 1 schematically illustrates this procedure for a region with two local SLP minima located at \mathbf{x}_1 and \mathbf{x}_2 , with $p(\mathbf{x}_1) < p(\mathbf{x}_2)$. For every minimum $p(\mathbf{x}_i)$ a set of contours $C_{i,j}$ ($j = 1, 2, \dots$) is determined with the contour values $p(C_{i,j}) = p(\mathbf{x}_i) + j \times \Delta p$, where Δp was set here to 2 hPa. Some technical details about the contour searching algorithm are given in the appendix. For the SLP minimum at \mathbf{x}_1 the contour $C_{1,n+1}$ is the first contour that encloses also the local minimum at \mathbf{x}_2 . Therefore $C_{1,n}$ is regarded as the

“outermost closed contour” for $p(\mathbf{x}_1)$ and the region bounded by $C_{1,n}$ (the gray shaded area in Fig. 1) corresponds to the cyclone L_1 with the central pressure value $p(\mathbf{x}_1)$. It is in this area that the cyclone field c is set equal to 1. The identified cyclone areas from simultaneously occurring cyclones do not overlap (see the examples in Figs. 2 and 3). Note that for weak cyclones it may be that no single closed contour can be found. In such a case the cyclone area is zero and the local SLP minimum identified in step (i) does not contribute to the cyclone field c . As will be discussed in section 6b, the choice of the contour interval Δp influences the number of cyclone centers for which at least one closed contour can be determined. This contour-based approach differs from the radial search algorithm introduced by Sinclair (1997) to determine the boundary of cyclonic airflow. Radial search (of a certain contour value or a change in the sign of the gradient) is assumed to work well for circular objects. The contour-based technique used in this study should lead to similar results for circular cyclones but might be more flexible in case of systems with a more complex shape.

The procedure is applied to all local SLP minima at every time instant of the ERA-40 dataset. Thereafter, the global cyclone field c (with values 0 and 1) is available every 6 h (cf. Fig. 2a) and can be used to build climatologies of surface cyclones by simple averaging of c over the time period of interest. The time-averaged cyclone field will be referred to as the cyclone fre-

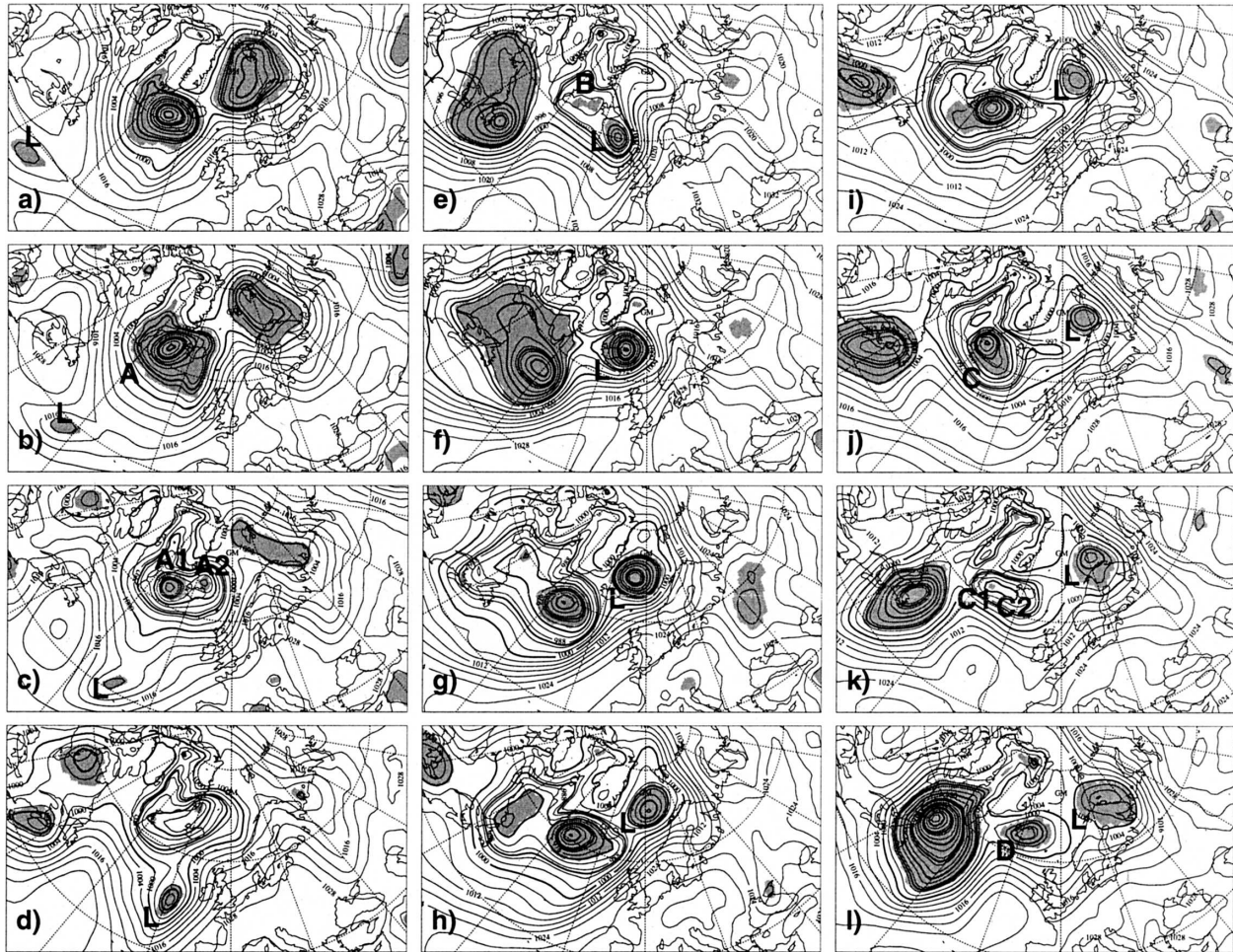


FIG. 3. Same as Fig. 2a but for the 6-day period from 0600 UTC 25 Feb to 1800 UTC 1 Mar 1992 and the Atlantic/European sector. Here only the identified cyclones are indicated by gray shading. The temporal separation between two panels is always 12 h. The SLP contour interval is 4 hPa.

quency field f_c . Its interpretation is straightforward, since it corresponds at every location to the percentage of time instants that the point is located within a cyclone. A value of $f_c = 20\%$, for instance, indicates that at this location a cyclone is present in 20% of the time during the considered overall period. Before presenting the climatological cyclone frequencies derived from the ERA-40 SLP fields in sections 3, examples are given in the next subsections to illustrate the adopted cyclone identification technique and to discuss its properties. Note as a side remark, that the same technique has also been applied to identify other features such as surface anticyclones when considering SLP maxima instead of minima.

b. An illustrative example

Figure 2a shows an example of the identified cyclones and anticyclones at an arbitrarily chosen date.

The darker gray shaded regions in Fig. 2a correspond to the cyclones (some of them labeled as L1 to L8) and the lighter shaded areas to the anticyclones (some of them labeled as H1 to H5) that have been detected by the algorithm. As described before, within these regions c or the analogously defined anticyclone field a are set equal to 1. The figure reveals that the algorithm captures almost all low- and high-pressure systems that are apparent from visual inspection. An exception is the very weak cyclone to the east of Florida at $\sim 30^\circ\text{N}$, where already the first SLP contour investigated, with a value that is 2 hPa larger than the local minimum, is not closed. Five depressions are present in the midlatitude Pacific Ocean: two cyclones (L1 and L4) of medium size in the western and eastern part, respectively, and three smaller cyclones (L2, L3 and one in the Bering Sea) in the central Pacific. Note that the algorithm is able to identify L2 and L3, which are relatively close to each

other and separated by a weak saddle point, as two separate features. The region extending from the North American to the Eurasian continent is characterized by a train of intense and large-scale cyclones and anticyclones (H1, L5, H2, L6, and H3). The two mature depressions L5 and L6 have a central pressure value of about 970 hPa. To the south of 40°N there is one larger system in the Mediterranean (L7), a small-scale cyclone in the subtropical Atlantic (L8), and many small-scale features over the United States, the central Atlantic, Mexico, and the Himalayan mountains. Some of them are probably spurious features due to significant extrapolation of the temperature field for the computation of SLP in high-mountain regions. For this reason, no cyclones will be determined from the SLP field in regions where the ERA-40 orography exceeds 1500 m.

It is instructive to compare the SLP field and the identified (anti)cyclones with the corresponding 1000-hPa relative vorticity field (Fig. 2b), which is characterized by significantly more small-scale features. On the one hand, some of the small-scale (anti)cyclones correspond directly to local vorticity extrema, for example L2, L3, L8, and H3–H5. On the other hand, the larger-scale cyclones (L1, L4–L7) are associated with complex large-amplitude vorticity patterns with multiple local extrema that, in some cases, are related to trailing fronts (see for example the vorticity filaments near the east coast of the North American continent and to the west of the United Kingdom). Further important differences can be seen for the continental anticyclone H1 and the probably spurious SLP structures in the high-mountain regions that have only weak signals in the vorticity field, and mainly in the subtropics where many vorticity extrema have no counterpart in the SLP field.

This example illustrates the ability of the algorithm to correctly identify the position and scale of cyclones and anticyclones in the SLP field. Using data with a horizontal resolution of about 1° also allows the identification of pressure systems that are comparatively weak and small-scale features with diameters of less than 500 km. A qualitative comparison of the pressure with the near-surface vorticity field indicates that for the relatively high-resolution ECMWF reanalysis datasets and without smoothing the fields (i) most of the identified pressure systems are associated with prominent vorticity structures, and (ii) that the abundant small-scale vorticity features would render a similar identification procedure based upon the relative vorticity field hardly practicable. However, for data with a coarser resolution, for instance from general circulation models, the vorticity field might be more appropriate for the identification of cyclones, in particular

in the early stage of their development, as suggested by Sinclair (1995) and Hodges et al. (2003).

c. An example episode

As a second example, an episode of 10 days is presented that features a cyclone (labeled L) with an exceptionally long lifetime that move from the western Atlantic via Scotland and the Barents Sea to western Siberia (Fig. 3). This serves to illustrate the routine's capability to reliably detect cyclones continuously along their track and to indicate some subtleties associated with cyclone identification and tracking. Cyclone L occurs first at 0600 UTC 25 February 1992 near 38°N, 53°W as a weak SLP minimum with about 1014-hPa central pressure (Fig. 3a). During the next 36 h it moves rapidly toward 20°W and intensifies slightly (Figs. 3b–d), followed by an explosive development with a pressure deepening from about 988 to 958 hPa within 24 h while passing Scotland (Figs. 3e,f). Then the cyclone weakens and slowly moves toward the Barents Sea (Figs. 3g–i) where it becomes quasi stationary with an almost constant size and amplitude (SLP minimum of ~990 hPa; Figs. 3j–l) for ~60 h. During its final phase (not shown), L moves over land and over the Ural into western Siberia. There it decays 10 days after its genesis near 66°N, 90°E. At all time instants of this long life cycle the algorithm captures the cyclone and its spatial extension. Some other features are noteworthy during this episode: 1) Cyclones can split, for instance near the southern tip of Greenland [Figs. 3b,c; see also the studies by Schwierz and Davies (2003) and Kurz (2004)]. Our algorithm identifies an intense cyclone A before (Fig. 3b) and two very small cyclones A1 and A2 just after the splitting. Cyclone tracking algorithms will regard A1 as the continuation of the former large cyclone A, and A2 as a newly formed cyclone. 2) Cyclones can merge, as shown for instance in Figs. 3e,f, where cyclone L absorbs a weaker cyclone B. In terms of cyclone tracking, this merging is interpreted as cyclolysis of B. 3) Cyclones can split and rapidly remerge, shown again for a cyclone near Greenland. In Fig. 3j, cyclone C is close to the southern tip, 12 h later (Fig. 3k) it has elongated into a structure with two local pressure minima and two tiny cyclones (C1 and C2) are identified that remerge within the next 12 h and form cyclone D (Fig. 3l). Such evolutions are particularly tricky for the tracking of cyclones and the question whether D is a continuation of C, or whether C decays into C1 and C2 develops into D cannot be answered unambiguously from the SLP field alone. These difficulties should be kept in mind when considering cyclone tracks and climatologies of genesis and lysis, and they illustrate the

value of a field like f_c that is independent from a tracking algorithm.

d. The tracking of synoptic systems

The procedure outlined in section 2a allows the production of climatological cyclone frequency distributions that will be shown in section 3. The combination of this cyclone identification with a tracking algorithm serves to obtain additional information about the depressions, like their location of genesis and lysis (see section 4), their lifetime and track length. Here a relatively straightforward tracking algorithm has been implemented that determines for a cyclone center at a certain time the most likely continuation among the identified cyclone centers 6 h later. Note that for this conventional tracking only the positions of the cyclone centers (i.e., the SLP minima) are taken into account and not the size of the cyclones as given by the outermost closed contours. A cyclone center located at \mathbf{x}_P at the time t_{n+1} is regarded as a possible candidate to continue the cyclone track $\mathbf{x}_Q(t_1), \dots, \mathbf{x}_Q(t_n)$ if the distance between $\mathbf{x}_P(t_{n+1})$, and the first guess location of \mathbf{x}_Q at time t_{n+1} , $\mathbf{x}_Q^*(t_{n+1})$, is less than a certain threshold distance $D = 1000$ km. The first guess location is calculated as a reduced linear continuation of the track in geographical longitude–latitude coordinates during the previous time step: $\mathbf{x}_Q^*(t_{n+1}) = \mathbf{x}_Q(t_n) + 0.75[\mathbf{x}_Q(t_n) - \mathbf{x}_Q(t_{n-1})]$. The factor of 0.75 is introduced because cyclone movement generally gets slower during a cyclone's life cycle. This parameter and the threshold value D are subjectively chosen and can be regarded as tuning parameters of the tracking algorithm. If two or more cyclones at time t_{n+1} are potential candidates to extend the cyclone track, then the cyclone that is closest to the first guess point is chosen. When searching the second point of a track, no previous displacement vector is available to estimate the first guess point. In this case the initial position of the cyclone is taken as the first guess.

Note that, similar to other tracking algorithms, our approach has significant caveats. They include the problem of the first tracking step (as described above) and the danger that short-lived systems are erroneously connected into longer-lived ones. For selected time periods, the technique has been subjectively validated and yielded satisfying results.

3. Climatological cyclone frequencies

a. The Northern Hemisphere

The seasonal mean cyclone frequencies f_c in the Northern Hemisphere (NH) are shown in Fig. 4. Recall

that the procedure to obtain f_c and its interpretation has been outlined at the end of section 2a. In the following, the main features of the seasonal cyclone frequencies f_c are described. Later, in section 6b, the results will be qualitatively compared with previous cyclone climatologies.

The dominant structures in the f_c field are the Pacific and Atlantic storm tracks with a clear seasonal cycle. In winter (December–February; DJF) bands with frequencies larger than 10% extend from Japan to the Gulf of Alaska, and from the North American east coast to the Barents Sea, respectively. Both storm tracks have two local maxima: in the central Pacific east of Kamchatka ($f_c \approx 35\%$) and in the Gulf of Alaska (with about the same amplitude); and in the Atlantic between Greenland and Iceland ($f_c \approx 32\%$) and in the Norwegian Sea ($f_c \approx 25\%$). In spring (March–May; MAM) the main structures are similar and the frequency values slightly smaller. Significant changes occur for summer and autumn. In summer (June–August; JJA) the main oceanic storm tracks are weaker and almost confined to latitudes north of 45°N . Local maxima with values of 20%–25% occur near the Aleutian Islands, Iceland, and over the Hudson Bay and Labrador area. In autumn (September–November; SON) the orientation of the principal storm tracks is more zonal than in winter and spring. In the Atlantic the structure is similar to summer, albeit with a larger amplitude. In the Pacific a pronounced maximum ($f_c > 35\%$) can be found in the Gulf of Alaska and a second (weaker) one in the Sea of Okhotsk. The latter feature occurs prominently during the fall season. Taking a closer look at Europe, it appears that over continental Europe f_c is largest in spring, over Scandinavia in summer, and over the United Kingdom in autumn. This is in contrast to the general North Atlantic cyclone frequency maximum in winter and indicates that Atlantic cyclones are less likely to move to the European continent in winter than during the warmer seasons.

Aside from the principal storm tracks, other midlatitude regions are also characterized by large cyclone frequencies, some with very strong seasonal variability. In the Mediterranean f_c attains peak values of about 15% during winter and of less than 10% in spring and autumn. In all seasons the largest values occur near Italy and in winter a secondary maximum is situated in the eastern Mediterranean. In contrast, in the Manchurian plain, east of the Altai–Sayan (50°N , 115°E) mountains, the maximum ($>16\%$) is in spring and the minimum in winter. Over North America, cyclones occur year-round, and for instance in the Great Lakes region with similar frequencies in all seasons.

Finally in the subtropics, our algorithm detects dis-

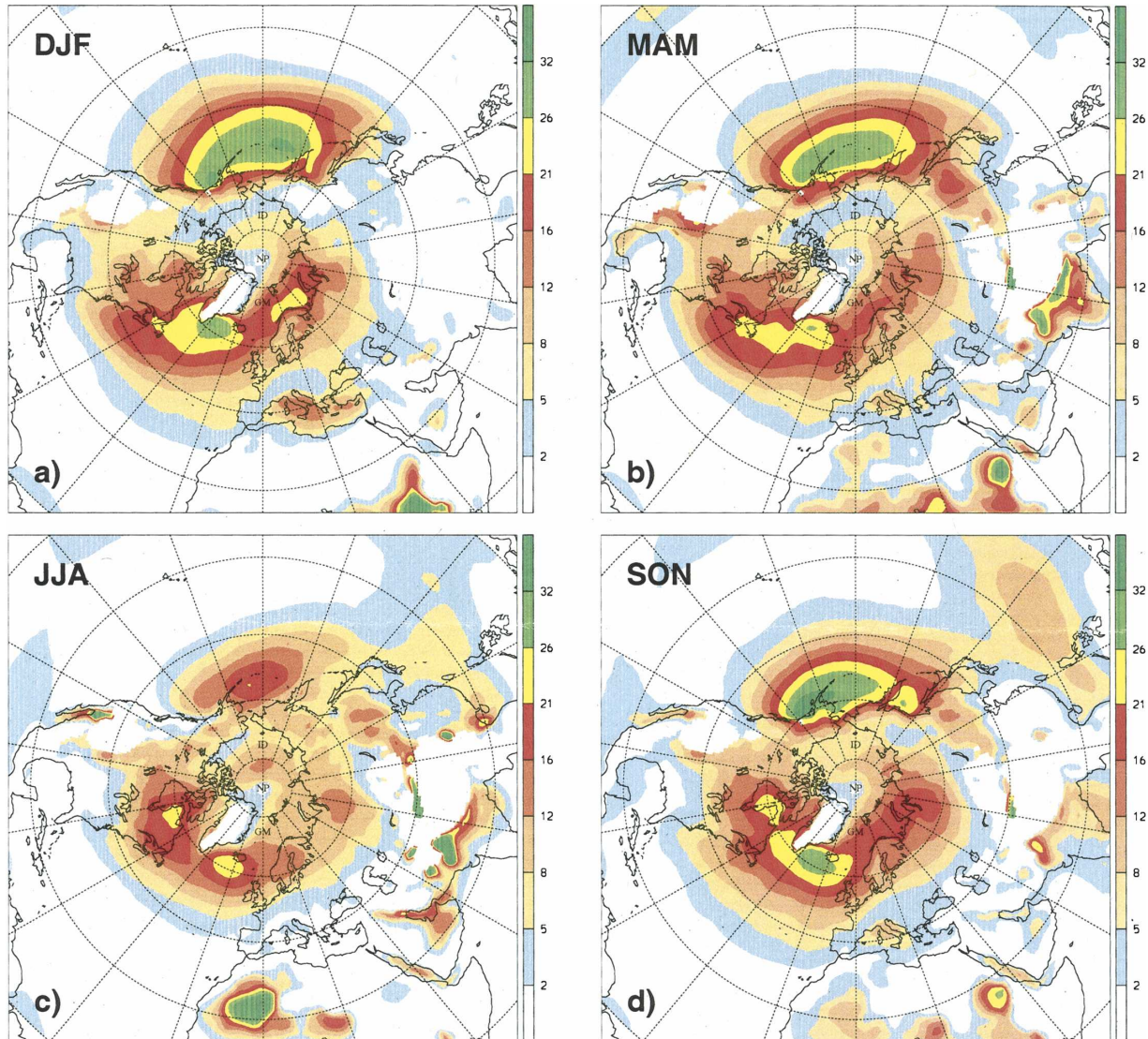


FIG. 4. Seasonal mean cyclone frequencies f_c (%) in the Northern Hemisphere for the ERA-40 period 1958–2001 for (a) DJF, (b) MAM, (c) JJA, and (d) SON. The field is not plotted in regions where the topography exceeds 1500 m.

tinct, large-amplitude maxima ($f_c \geq 30\%$) of cyclone frequencies, for instance in DJF, MAM, and SON over eastern Africa in the upper Nile region, in JJA over the western Sahara, in MAM and JJA over Pakistan and northern India and also mainly in JJA near Baja California. Lower amplitude maxima ($f_c \approx 10\%$) occur mainly in MAM over northern Africa and in JJA over the Red Sea and the Persian Gulf. Also in JJA and more pronounced in SON, cyclone frequencies are enhanced (peak values of about 10%) in the South China Sea and in the Pacific east and north of the Philippines. This area is known to be a region with frequently occurring tropical storms (Emanuel 2003). In general however, these prominent subtropical maxima of f_c do

not contain any information about the depth or intensity of these cyclones. For instance, during DJF, their minimum SLP value very rarely falls below 1000 hPa (not shown).

b. The Southern Hemisphere

Seasonal mean cyclone frequencies for the Southern Hemisphere (SH) are shown in Fig. 5. They are strikingly different from their NH counterparts. Between about 55°S and the coast of Antarctica, a band with f_c values of 20%–40% extends zonally around the entire hemisphere with a break near the Antarctic Peninsula. This distinct structure has three local maxima near 30°E , 100°E , and 140°W , and its intensity is almost con-

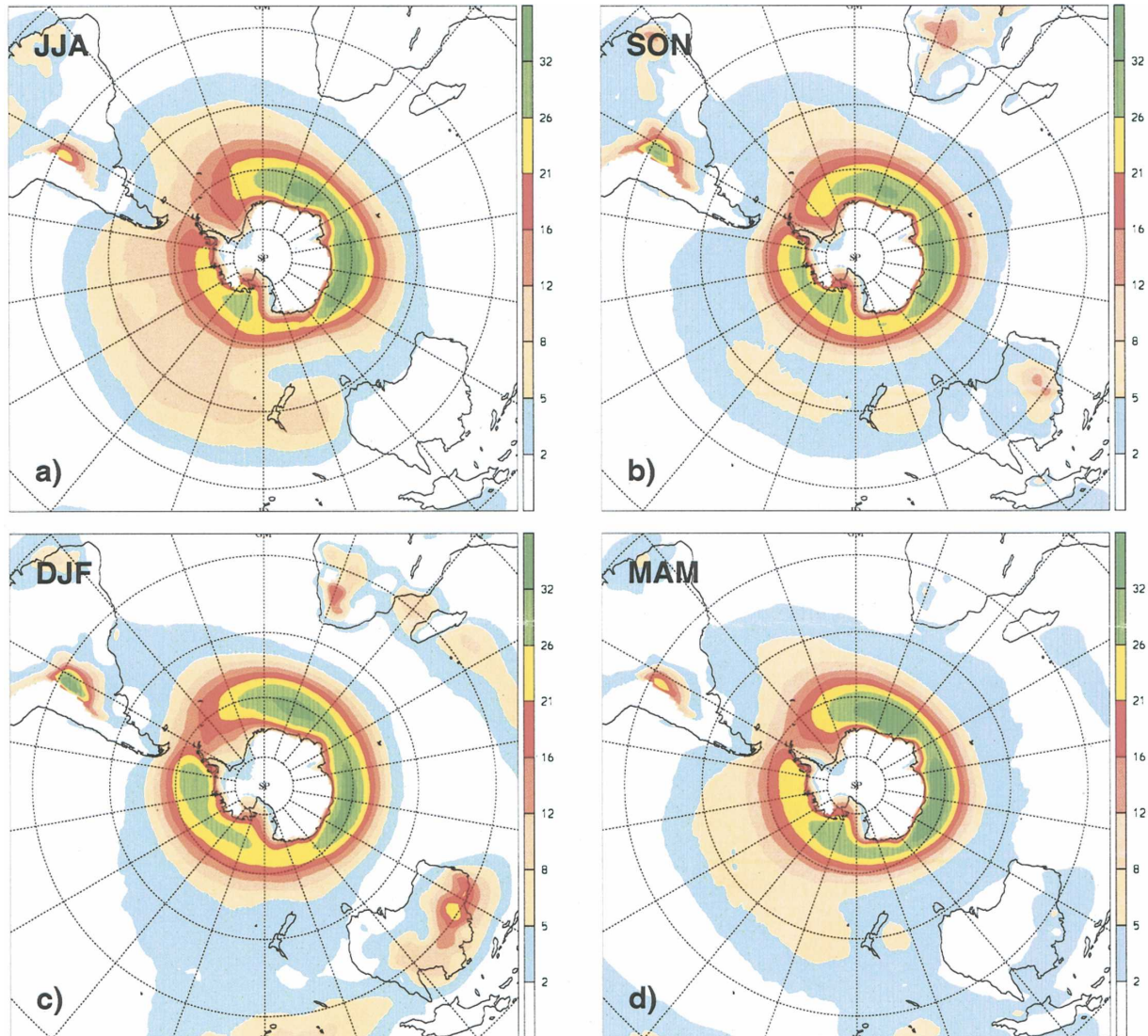


FIG. 5. Same as Fig. 4 but for the Southern Hemisphere for the ERA-40 period 1958–2001 for (a) JJA, (b) SON, (c) DJF, and (d) MAM. The field is not plotted in regions where the topography exceeds 1500 m.

stant throughout the year. Farther equatorward, between 30° and 60° S, cyclones occur in the South Pacific with peak frequencies of about 10% during winter (JJA), and less frequently and with a weaker seasonal cycle in the South Atlantic. The winter Pacific cyclones form a band that extends zonally from southeast Australia to Patagonia. In contrast, the Atlantic region with enhanced cyclone frequencies extends southeastward from the South American east coast and merges with the more prominent band around Antarctica. In the subtropics, a prominent maximum of f_c exists in all seasons near 25° S over northern Argentina, with largest amplitude ($f_c > 30\%$) in summer (DJF) and spring (SON). In the same two seasons there are continental

maxima of cyclone frequency over northwest Australia and southern Africa. Only in summer two subtropical marine areas also reach f_c values of almost 10%, one east of Africa and Madagascar, and the other east of Australia and over the Fiji Islands. Here again, our algorithm seems to identify tropical storms, as indicated by a qualitative comparison with Emanuel (2003, his Fig. 1).

4. Genesis and lysis of cyclones

Here the geographical distributions of the points of cyclogenesis and cyclolysis are presented for both hemispheres during the contrasting winter and summer sea-

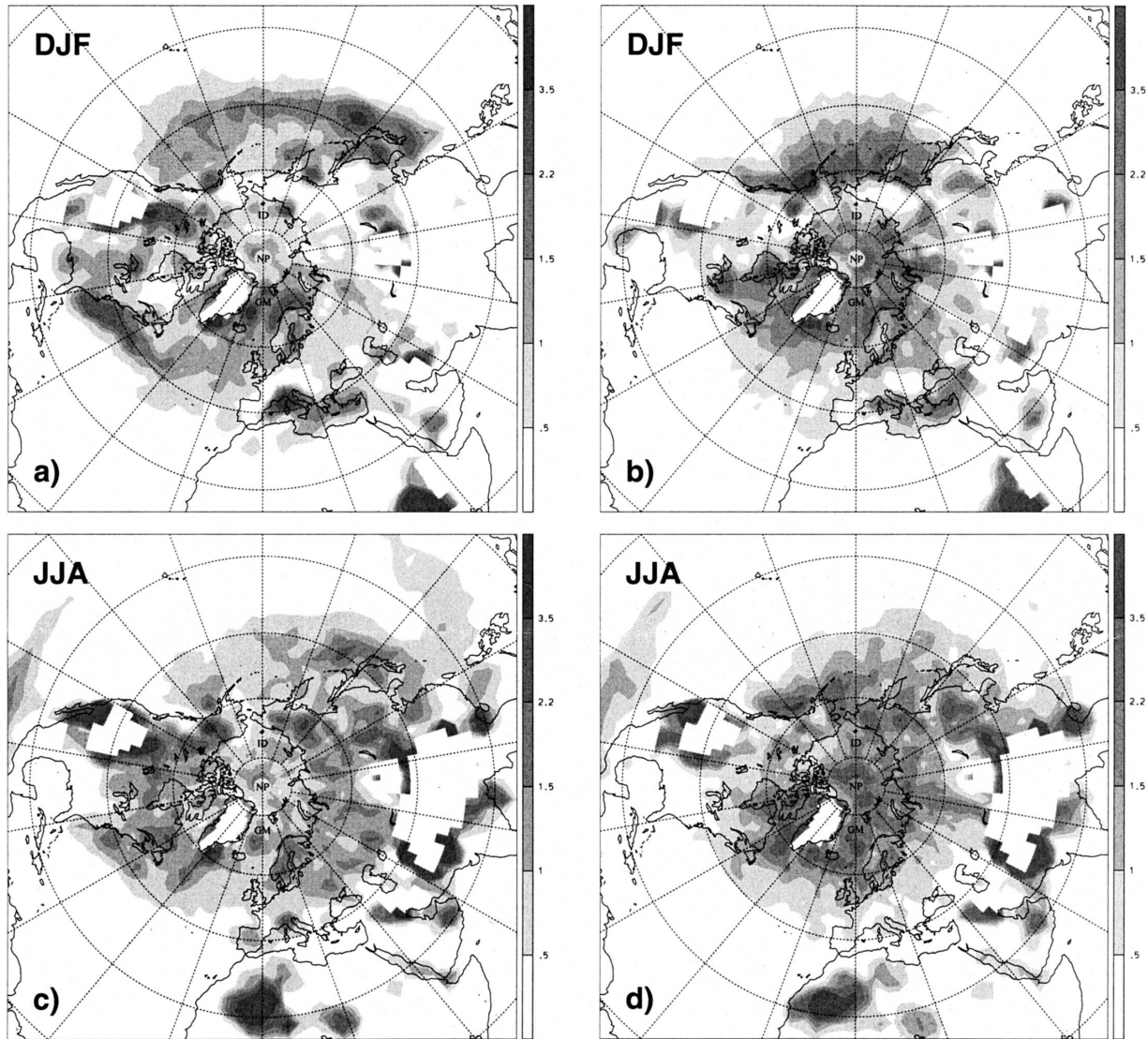


FIG. 6. Seasonal climatologies of Northern Hemisphere (a),(c) cyclogenesis and (b),(d) cyclolysis for the time period 1958–2001 for (a),(b) winter (DJF) and (c),(d) summer (JJA). The units are number of events per 10^4 km². The field has been calculated on a $3^\circ \times 3^\circ$ grid and is not plotted in regions where the topography exceeds 1800 m.

sons. Recall that the location of genesis and lysis corresponds to the initial and final point of a cyclone track and therefore the following results, in contrast to the cyclone frequency fields, depend upon the details and the parameters of the tracking algorithm (cf. section 2d).

a. The Northern Hemisphere

Figure 6 shows the results for NH cyclones with a track life time of at least 1 day. During winter (Fig. 6a), cyclogenesis is most frequent in the western Pacific (at 30° – 40° N) with three local maxima in the Japan Sea, southwest and east of Japan, respectively, and in the

western Atlantic (at 32° – 41° N) along the U.S. east coast from South Carolina to Massachusetts. A third major region of cyclogenesis is located in the western Mediterranean near the Gulf of Genoa (40° – 44° N). Despite the pronounced maxima in the western oceans, it is important to note that cyclogenesis occurs across the entire Pacific and Atlantic north of about 35° N. Additional localized maxima of cyclogenesis with weaker amplitude appear for instance in the lee of Altai-Sayan, west and east of Kamchatka (55° N, 165° E), in the Gulf of Alaska (57° N, 145° W), east of the Rocky Mountains, in the Great Lakes and Mississippi area, east of the southern tip of Greenland, north of Iceland, east of

New Siberia Islands (70°N, 155°E), north of Scandinavia, and in the eastern Mediterranean.

Most of the winter genesis regions remain valid also for the summer season (Fig. 6c), although often with weaker amplitudes. Major differences occur however in the Mediterranean (much reduced cyclogenesis in summer) and over Labrador, Kazakhstan, east of the Lake Baikal and in eastern Siberia (with strongly increased cyclogenesis in summer). Also in the subtropics several regions appear in summer as active areas of cyclogenesis. These cyclones are typically stationary features as shown by the summer distribution of cyclolysis (Fig. 6d) that, in the subtropics, looks very similar to the distribution of genesis. It is likely that many of these systems over the continents are heat lows that are recreated almost daily and therefore lead to strong coinciding signals of genesis and lysis. An exception is the genesis region in the western subtropical Pacific (10°–20°N, 110°–150°E). These cyclones are moving away from their genesis region as there is no signal of lysis in the same area.

Cyclolysis in the extratropics (Figs. 6b,d) is most frequent in the northern Pacific (50°–62°N, with a local maximum in the Gulf of Alaska), in the Hudson Bay and Great Lakes area, in the central Atlantic near the southern tip of Greenland, in the eastern Mediterranean (only in winter), east of the Ural, and over Manchuria. The two prominent regions of wintertime cyclogenesis in the western parts of the North Pacific and North Atlantic are associated with very little cyclolysis, indicating that cyclones created in this area generally move rapidly away from their region of origin.

b. The Southern Hemisphere

Figure 7 shows the winter and summer distributions of the points of genesis and lysis of surface cyclones (with a lifetime of at least 1 day) in the SH. During winter (JJA; Fig. 7a), cyclogenesis is most frequent in the region close to Antarctica near 60°S and in distinct midlatitude areas near 30°–40°S. They comprise mainly the regions just off the east coasts of South America, Australia, and New Zealand. The area between 40° and 60°S is characterized by a fairly low and almost uniform rate of cyclone formation. The Antarctic ring of genesis resembles the cyclone frequency field (Fig. 5), except for the region in the lee of the Antarctic Peninsula, which shows high values of genesis (Fig. 7a) but low values of cyclone frequency and lysis (Fig. 7b). The distribution of lysis reveals large values all along the coast of Antarctica. A particular maximum of cyclolysis is located upstream of the west coast of Chile, where the southern Andes are a significant obstacle for propagating cyclones.

During summer (Fig. 7c) genesis is slightly less frequent in higher latitudes (40°–80°S) compared to winter, but more frequent in certain subtropical areas over and to the east of Africa, Australia, and South America. Most of these systems, in particular the ones over land, are quasi stationary as revealed by the similarity of the fields of cyclone frequency, genesis (Fig. 7c), and lysis (Fig. 7d) in these areas. An exception is the cyclones that originate to the east of South America (Fig. 7c). As during the winter season, they move poleward and, according to the difference between Figs. 7c and 7d, it can be speculated that some of them decay east of the Greenwich meridian. Such links between areas of genesis and lysis will be firmly established for selected regions in the next subsection.

5. Cyclones in selected geographical regions

In the previous sections, the regions of frequent cyclone occurrence, genesis, and lysis were presented separately. Here, the techniques to determine cyclone frequency fields and cyclone tracks are combined in order to investigate quantitatively and in detail the behavior of cyclones in some selected regions. The motivation for such an analysis is twofold. First, the results presented so far provoke questions on the origin of cyclones that contribute to a certain local cyclone frequency maximum, or on the typical end points of cyclone tracks that originate in a certain region of genesis. Second, focusing on cyclone subsets with a certain area of genesis, lysis, or passage can point to important regional differences in the behavior and dynamics of extratropical cyclones. HH02 already showed similar cyclone subset analyses, namely lysis and genesis densities for selected genesis and lysis regions, respectively (their Fig. 7). Figure 8 now serves to introduce and illustrate our approach to construct and visualize specific cyclone subsets. For this example, winter cyclones with a lifetime of at least 24 h have been selected that originate in the western North Atlantic. This region, referred to as ATLwest in the following and shown as a box outlined in black in Fig. 8b, has been identified as a key region of cyclogenesis (cf. Fig. 6a). The ATLwest cyclone subset is shown in four different ways, and the advantages and disadvantages of the various visualizations will be briefly discussed. In the following subsections, one type of representation will be used to present other cyclone subsets in both hemispheres.

Figure 8a shows the tracks of all ATLwest cyclones during the 44 DJF seasons. Their total number is 599, or about 4–5 tracks per winter month. The initial and final points of the tracks correspond to the location of gen-

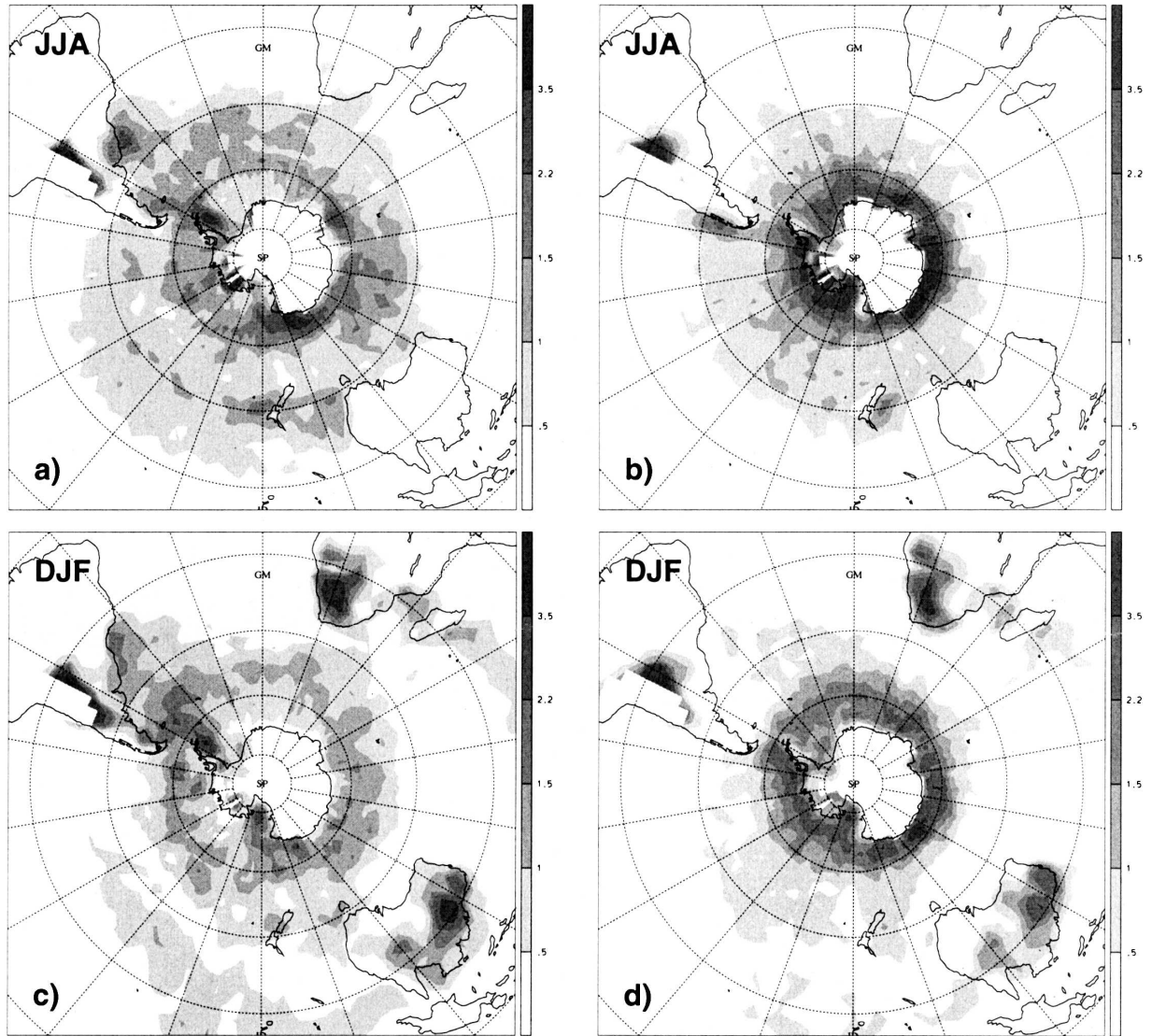


FIG. 7. Same as Fig. 6 but for Southern Hemisphere (a),(b) winter (JJA) and (c),(d) summer (DJF).

esis and lysis, respectively, and the areas crossed by the cyclone track in between genesis and lysis will be referred to as areas of cyclone passage. The cyclone tracks are very dense in the oceanic region between 40° and 70°N , indicating a general east/northeastward movement of ATLwest cyclones. In the regions to the south, north, and east of the principle storm-track area, the pathway of individual cyclones and their location of lysis become apparent. A few ATLwest cyclones move, for instance, into the subtropical North Atlantic or the Mediterranean, and others across the North and Baltic Seas toward Eastern Europe or on either side of Greenland into the Arctic. The density of these cyclone tracks is plotted in Fig. 8b. This visualization does not allow one to follow individual tracks but provides a quantifi-

cation of the track frequency in the major storm track area. However, both Figs. 8a and 8b do only consider the centers of the ATLwest cyclones and are therefore not directly comparable to the overall cyclone frequencies (Fig. 4a). Therefore, a subset of the frequency field f_c has been calculated that considered only the selected ATLwest cyclones (Fig. 8c). Because now the cyclones are again regarded as finite regions, the area with a nonzero amplitude is slightly enlarged compared to the track density field shown in Fig. 8b. This ATLwest subset of f_c has the same units and can be directly compared to the total cyclone frequency field (Fig. 4a). For instance, the maximum values of almost 10% off Newfoundland indicate that in 10% of the wintertime instants a cyclone is present in this region that has origi-

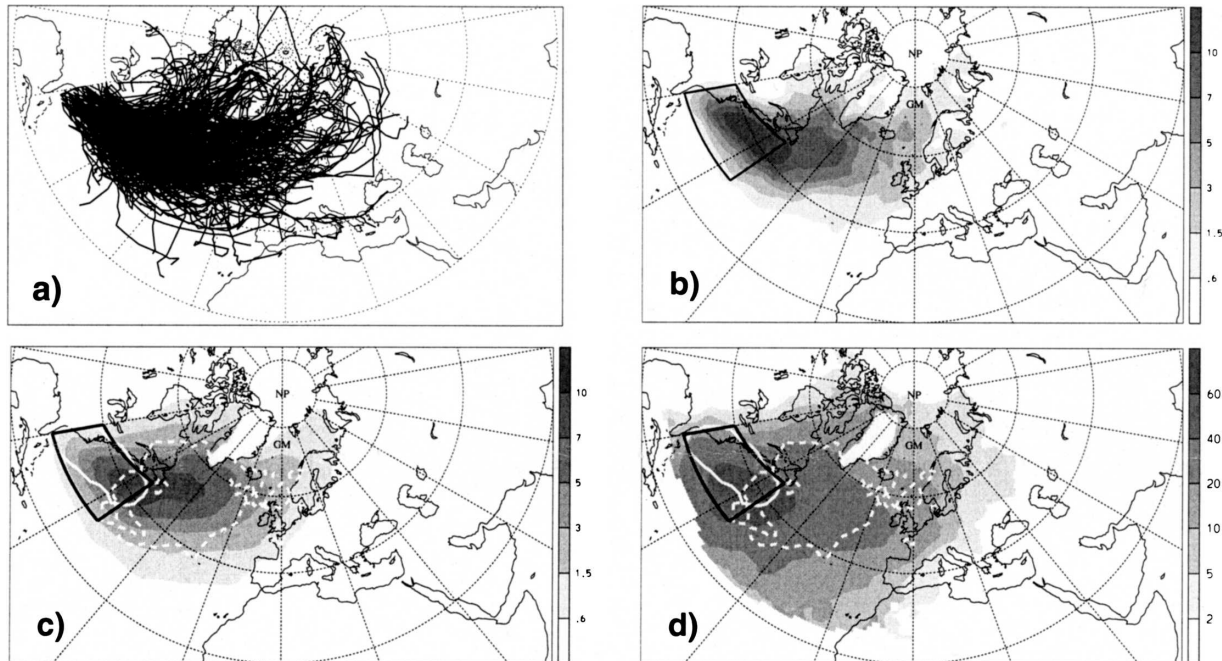


FIG. 8. Different visualizations of DJF cyclones with genesis in the western North Atlantic [see black box in (b)–(d)]. (a) The individual cyclone tracks, (b) the track density field (in number of 6-hourly track points per 10^4 km 2), (c) the absolute, and (d) the relative cyclone frequency field r_c (%). Overlain in (c) and (d) are white contours that indicate the regions of enhanced genesis (solid line) and lysis (dashed line) of these cyclones.

inated in the ATLwest area. For Ireland and Scotland this value reduces to less than 3% and comparison with the much larger values of f_c in Fig. 4a (which shows all cyclones independent of their location of genesis) elucidates that other genesis regions contribute strongly to cyclones near the British Isles.

This fact is brought out more clearly in Fig. 8d, which shows the relative cyclone frequency field, r_c , the ratio of the cyclone frequency field subset (Fig. 8c), and the total f_c (Fig. 4a). (No values are plotted in regions where the total f_c is insignificant, i.e., less than 0.5%.) This field is interesting because it provides quantitative information about the relative importance of the ATLwest genesis region for the cyclone frequency in other areas. It is relative to the total cyclone frequency field, so it responds to questions about the percentage of all cyclones in region X that originated in region Y, but it does not reflect how many cyclones originating in region Y reach region X. In the western Atlantic ($r_c \sim 50\%$) about every second cyclone has originated in the specified area. In almost the entire Atlantic area, including the U.S. east coast, Newfoundland, the Labrador Sea, Iceland, the United Kingdom, Benelux, and northwest France, r_c is larger than 20%. For areas more remote from the origin, for instance, in the western Mediterranean, in Central Europe, in western Russia and the Barents Sea, r_c is much smaller but still

amounts to 2%–5%. This is in qualitative agreement with Fig. 8a showing that a few cyclone tracks that start in the ATLwest region reach the Arctic or Europe, but now in Fig. 8d the information is quantitatively put in relation to the overall cyclone frequency field. As additional information, the overlaid contours in Figs. 8c,d indicate the areas where the considered ATLwest cyclones most typically undergo genesis and lysis (the contour values have been chosen as 20% of the local maximum values of the ATLwest subset genesis and lysis fields, respectively). As a caveat it is noted that in particular Fig. 8d does not indicate the typical pathways of cyclone centers. It is for instance not clear whether the ATLwest cyclones that reach the United Kingdom do so by crossing the Atlantic at more northerly or southerly latitudes.

This example of the ATLwest subset of cyclones indicates the value of such detailed considerations of certain areas of cyclone genesis, passage, and lysis, and has introduced the relative cyclone frequency field r_c and its qualities. This field will now be used to investigate different regions of cyclone genesis, passage, and lysis during the winter season that were regarded as particularly interesting, based upon the climatological results (Figs. 4–7). The results for the different regions are presented in Figs. 9–11 and discussed in the next subsections.

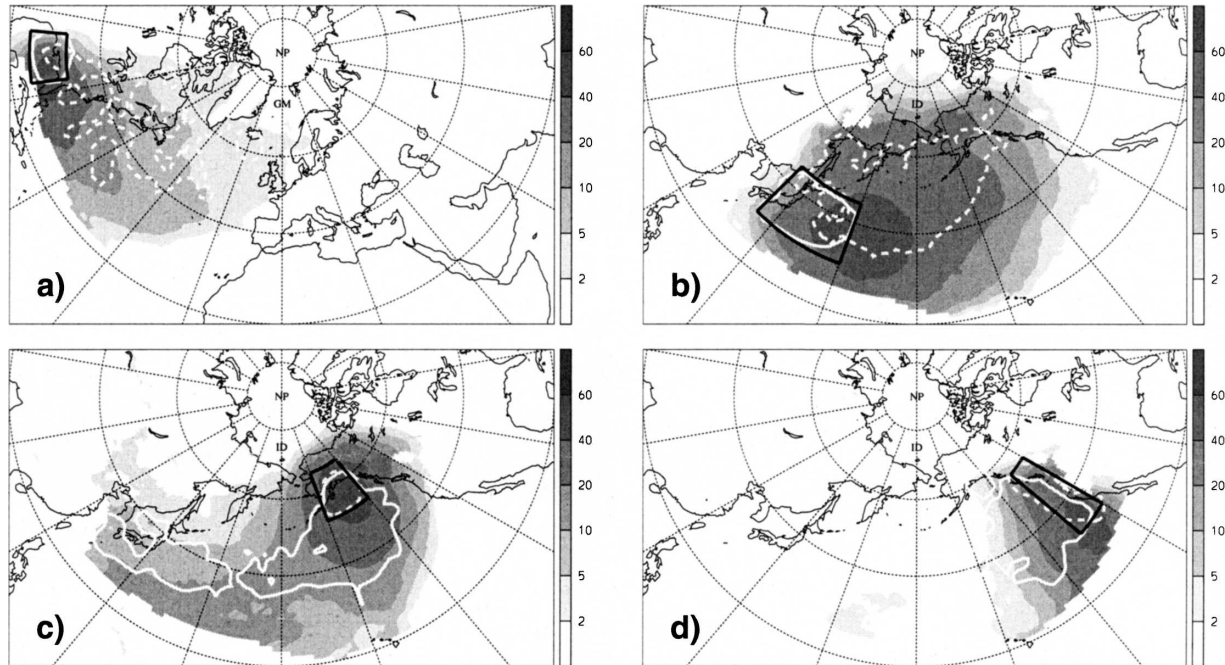


FIG. 9. Relative cyclone frequency field r_c (%) during DJF for cyclones with (a) genesis near the U.S. southeast coast, (b) genesis in the western Pacific, (c) lysis in the Gulf of Alaska, and (d) lysis along the U.S./Canadian west coast. Overlain are white contours that indicate the regions of enhanced genesis (solid line) and lysis (dashed line) of these cyclones.

a. Northern Hemisphere subregions

Cyclones from the southern United States (Fig. 9a; USsouth) are of particular importance for the southeastern United States and the western North Atlantic south of 40°N ($r_c > 20\%$). Some of them reach Iceland and the United Kingdom where they contribute 2%–5% to the total cyclone frequency field. Cyclolysis of these systems occurs in several areas, in the southern United States, near Newfoundland, and Iceland.

Cyclones with genesis east of Japan (Fig. 9b; JAPeast) are relevant for the entire North Pacific, similar to the importance of the ATLwest cyclones for the North Atlantic (cf. Fig. 8d). In the region between Japan, Alaska and the central Pacific, about every second cyclone originates in JAPeast. Along the U.S. west coast, the r_c values decrease from 50% in Alaska to 10% near Vancouver Island and about 2% in California. Thus, many of these cyclones move in northeastward direction as far as the Gulf of Alaska but only few of them reach the U.S. west coast where systems with other genesis regions must be more important. Lysis of the considered cyclones is almost equally likely over the entire central Pacific. Qualitative comparison with Fig. 7a of HH02, who presented the lysis density for genesis in the western North Pacific, yields reasonable agreement.

It is now interesting to complement the above “for-

ward” perspective of the North Pacific storm track with a “backward” investigation of the origin of cyclones that arrive at the U.S. west coast. This is done both for the Gulf of Alaska region (Fig. 9c; GAL) and further south for the U.S./Canadian west coast between 30° and 55°N (Fig. 9d; USwest). Cyclones with tracks that end in GAL can be categorized into three groups: (i) stationary cyclones, (ii) east Pacific cyclones with genesis some 2000 km south-southwest of the Gulf, and (iii) systems with long-distance tracks from the western Pacific. Five to ten percent of the cyclones near Japan will undergo lysis in the Gulf of Alaska. For eastern China and Kamchatka this number is smaller (2%–5%) but nevertheless indicates the existence of very long Pacific cyclone tracks that originate over the Asian continent (cf. Fig. 6a). Cyclones that experience lysis in USwest have very different tracks compared to the ones that end in GAL. Almost all of them originate from the eastern North Pacific (east of 150°E) and the GAL area, in agreement with Fig. 7b in HH02.

Next, cyclone tracks are investigated that pass through eight specific regions of interest (Fig. 10). Cyclones that move across the cyclone frequency maximum in the central Pacific (Fig. 10a; PACmax) are slightly different from the ones for JAPeast (Fig. 9b). Some of their tracks start further upstream in the Japan Sea or even over Manchuria, others to the east of

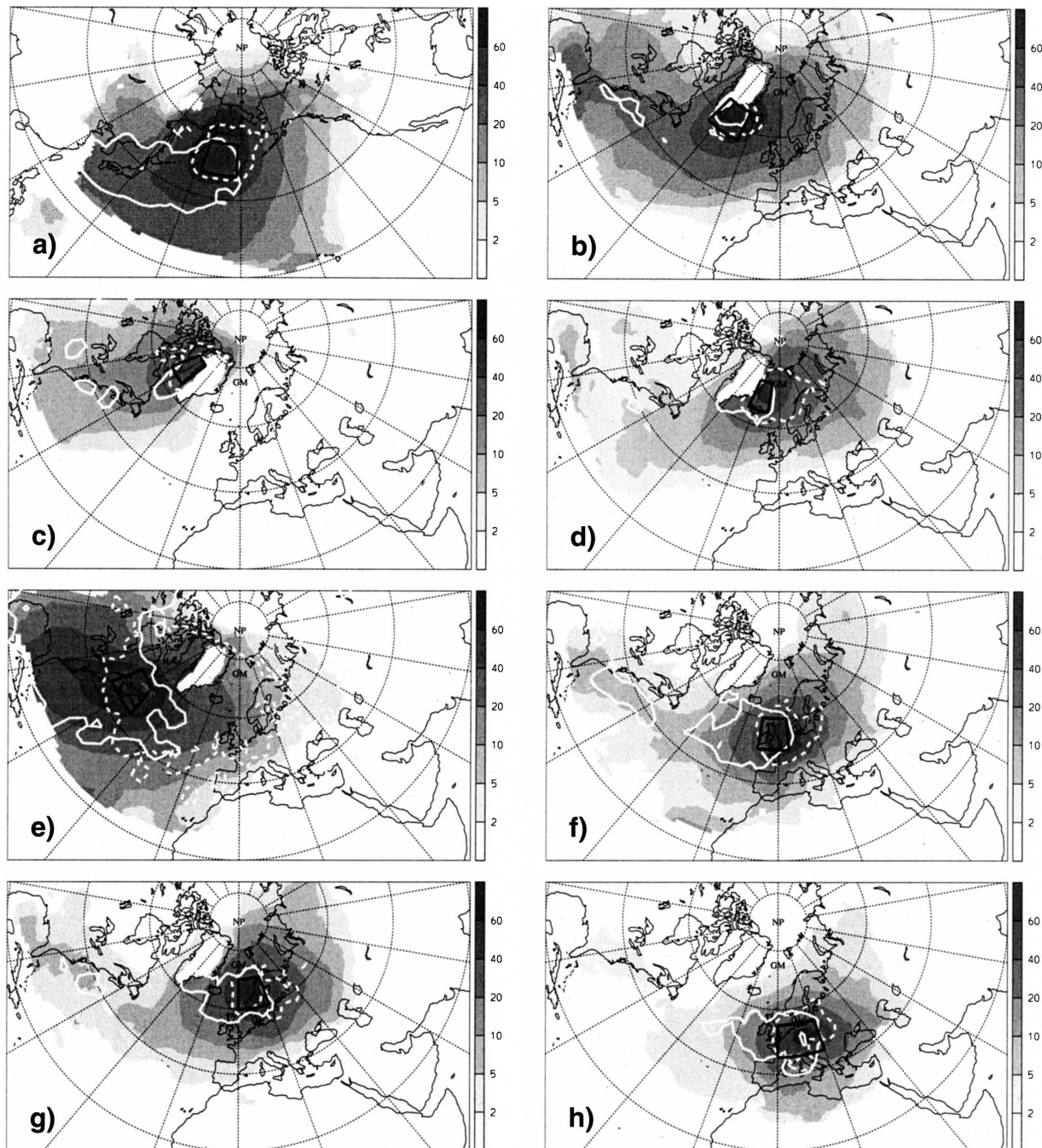


FIG. 10. Same as Fig. 9 but for cyclones with tracks that intersect (a) the central North Pacific, (b) the central North Atlantic, (c) the west coast of Greenland, (d) the east coast of Greenland, (e) Newfoundland, (f) the British Isles, (g) Scandinavia, and (h) central Europe.

Kamchatka. They contribute very little to western U.S. cyclones, indicating that cyclones that reach the western United States originate further downstream (cf. Fig. 9d) or cross the central Pacific south of the cyclone frequency maximum.

Cyclones that move through the North Atlantic

maximum of f_c (Fig. 10b; ATLmax) contribute to the cyclone frequency field in a very large area from eastern America to Russia. Twenty to forty percent of the cyclones that affect Florida, Newfoundland, the United Kingdom, and Scandinavia move through this region. The considered cyclones originate preferentially along

the North American east coast but also over the central and eastern United States and near the southern tip of Greenland.

Cyclones that move along the Greenland west and east coast are visualized in Fig. 10c (GLwest) and Fig. 10d (GLEast), respectively. Their tracks differ significantly. The former category is much more prominent over Canada and nonexistent in the eastern North Atlantic. East of the Greenwich meridian, the frequency field of the GLEast category looks similar to the one for ATLmax (Fig. 10b), but the GLEast cyclones rarely originate from the eastern Atlantic. Interestingly, from all cyclones over the eastern United States and Canada and off the southern United States east coast, 5%–20% move to the Greenland west coast, but only 2%–5% to the east coast. Note that the figures do not indicate the direction of the cyclone tracks. However, a more detailed investigation of the areas of genesis and lysis shows for instance that most of the GLEast cyclones that also affect the United Kingdom move from GLEast to the United Kingdom and not vice versa.

Cyclones that cross Newfoundland (Fig. 10e; NFL) mainly originate along the eastern American coast. Their effect on Europe is relatively small compared to the ATLmax and GLEast cyclones. However, they have a significant influence on f_c in the subtropical eastern North Atlantic.

Cyclones that move across the United Kingdom (UK), Scandinavia (SKA), and Central Europe (CEU) are shown in Figs. 10f,g,h, respectively. For all categories cyclogenesis occurs frequently in the eastern North Atlantic, which indicates the relevance of secondary genesis for European landfalling cyclones. They are also similar in their contribution to f_c in Eastern Europe and Russia. There are also interesting differences. Some of the SKA and UK cyclones originate in the western North Atlantic whereas CEU cyclones do so only very rarely. A few cyclones from the subtropical eastern Atlantic arrive at the United Kingdom but not in the two other areas. Also, a significant part of the CEU tracks start in the Gulf of Genoa whereas the SKA cyclones are (almost) confined to the region north of the Alps. However, the latter penetrate more frequently into northern Eurasia.

b. Southern Hemisphere subregions

Polar cyclones with genesis in the lee of the Antarctic Peninsula (Fig. 11a; ANTpen) and subtropical cyclones with genesis in the Tasman Sea (Fig. 11b; TAS) do typically not move very far. However, a small number (~5%) of the cyclones that reach Chile near 50°S have crossed the entire South Pacific.

Cyclone tracks that originate from the east coast of

South America near 30°S (Fig. 11c; SAMEast) are highly variable. The majority decays within a distance of 2000 km from the coast, but a significant part moves poleward and reaches the eastern Antarctic coast where they contribute up to 10% to the cyclone frequency field. Cyclones with tracks that end along the Chilean coast (Fig. 11d; SAMwest) mainly originate from the eastern Pacific near 40°S but some tracks extend back to New Zealand.

Cyclones with lysis along the west and east coast of Antarctica are shown in Fig. 11e (ANTwest) and Fig. 11f (ANTeast), respectively. ANTwest cyclones are present in the entire west Pacific, from 25° to 80°S. They originate mainly from southern latitudes but also from the subtropics and in some cases even from the subtropical Atlantic. Similarly, ANTeast cyclones contribute 10% or more to f_c in a large part of the Atlantic. Their genesis regions are widely distributed and include the South American east coast and in some exceptional cases the South Australian Basin. Such extremely long tracks of more than 180° longitude, according to our tracking procedure, occur only in the SH. With the aid of time sequences of SLP charts we verified that these long tracks have been correctly identified by the algorithm.

6. Discussion

a. Caveats of the method

As mentioned above, the method introduced in section 2 considers the size of a surface cyclone, where the size is taken as the area within closed SLP contours. This approach is meant to be in line with the traditional approach of cyclone identification from surface synoptic charts. It is therefore conceptually straightforward, although technically elaborated. However, there are some important caveats of the method and its application to SLP data.

First, cyclones must be associated with a local SLP minimum in order to be identified by the algorithm. In the case of a weak ambient flow field, a northern hemispheric vorticity maximum might be associated also with a local SLP minimum. In contrast, in the case of a strong ambient flow the SLP signature associated with a vorticity maximum is possibly a low-level trough without closed contours. This implies that vorticity could be a better variable than SLP or low-level geopotential height to identify surface cyclones in their early stage, as proposed by Sinclair (1995) and Hodges et al. (2003). In these studies data with a relatively coarse resolution has been used (2.5° and truncation to T42, respectively). However, when using datasets with a horizontal resolution of 1° or less, the near-surface vorticity field

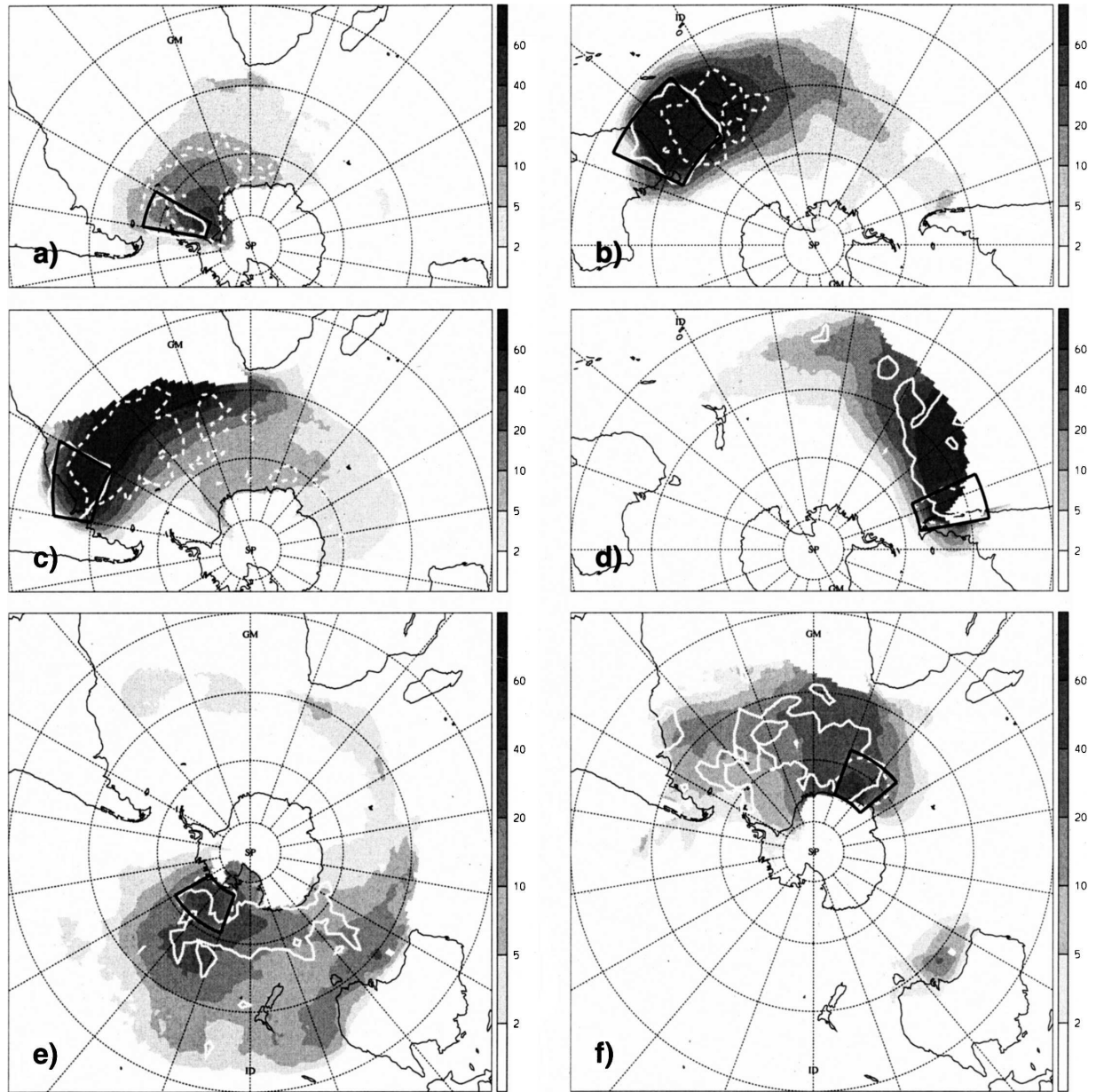


FIG. 11. Same as Fig. 9 but during JJA for cyclones with (a) genesis in the lee of the Antarctic Peninsula, (b) genesis in the Tasman Sea, (c) genesis in the region off the South American east coast, (d) lysis along the Chilean coast, (e) lysis along the west coast of Antarctica, and (f) lysis along the east coast of Antarctica.

contains many small-scale features (cf. Fig. 2) and a clear and simple relationship with cyclones is lacking as noted also by Sickmüller et al. (2000) and Hanson et al. (2004). An alternative to minimize the influence of the ambient flow on the cyclone identification would be to use suitably defined SLP anomaly fields instead of the full SLP field. The same technique as used here could be applied directly to anomaly fields and it would be interesting to compare the results.

Second, the size of a cyclone as defined here is sen-

sitive to the occurrence of other SLP minima in the neighborhood and in some cases can fluctuate strongly in time. Such a situation was shown in Fig. 3 where a large, mature cyclone splits into two much smaller cyclones, conceivably by interaction with the Greenland topography. In some cases the splitting is not permanent. The two SLP minima can merge and the cyclone area enlarges again. Such fluctuations of the cyclone size have an impact on the climatological cyclone frequency field f_c but they do not necessarily reflect a

change in the dynamics or intensity of the cyclone. It is purely an effect of the SLP topology and is a caveat that does not occur with classical cyclone climatologies that do not consider the size of the depressions. Nevertheless, the typical cyclone sizes determined by the contour searching technique, agree fairly well with other size estimates of cyclones. For instance Simmonds (2000) calculated the temporal evolution of the averaged cyclone radius throughout their life cycle and found an increase of the mean radius from about 500 km at day 0 to 600–700 km at day 4. Considering cyclones as circles (for simplicity), the same averaged time evolution has been calculated from the cyclone sizes as determined by our contour algorithm. The results show an increase from about 350 km to more than 800 km between days 0 and 4. The smaller values at the time of genesis might be due to the higher data resolution (1° versus 2.5° used by Simmonds), while the larger value after 4 days might be due to the differing definitions of cyclone radii. This assessment illustrates that the potential problems mentioned above do not lead to systematically smaller cyclone areas. Also, the approximate doubling in scale during the initial 4-day development is consistent with the case studies of North Pacific cyclones performed by Grotjahn et al. (1999).

Third, the contour interval Δp is a tunable parameter of the introduced cyclone identification technique. All results shown have been obtained with a value of $\Delta p = 2$ hPa. Sensitivity studies with values of 1, 3, and 4 hPa (not shown) yielded the following results. The absolute number of identified cyclones depends strongly on to this parameter. It increases by about 40% if changing Δp from 2 to 1 hPa and it decreases by 30% if changing Δp from 2 to 4 hPa. However, the additional cyclones that are found for a smaller value of Δp are typically weak (i.e., their minimum SLP is almost equal to the neighboring grid points) and small. They do not contribute strongly to the climatological cyclone frequency field and the geographical patterns shown in Figs. 4 and 5 are in essence unaffected by the choice of this parameter. The same holds for the geographical distributions of genesis and lysis. Although the number of cyclones changes when varying Δp , this does not affect the location of the preferred regions for cyclogenesis and cyclolysis.

And finally, the resulting cyclone frequency field is sensitive to the resolution of the underlying model and SLP dataset. A model with a relatively coarse resolution, for instance a GCM with a resolution of 2° to 5° , produces less small-scale cyclones. Therefore, according to the caveat mentioned above, mature cyclones are identified with a larger area than in a high-resolution dataset that potentially contains additional local SLP

minima. This implies that quantitative intercomparisons of cyclone frequencies using different datasets or models should be based, if possible, on fields with equal horizontal resolution. This issue of sensitivity to the data resolution is, however, not specific to the technique used in this study but pertains also to more conventional cyclone tracking studies (Blender and Schubert 2000; Zolina and Gulev 2002).

b. Comparison with previous cyclone climatologies

In a qualitative way, the results from this study (cyclone frequency fields and regions of genesis/lysis) can be compared to previous cyclone climatologies that are often based on a tracking algorithm and represent cyclones by their point of minimum SLP or maximum relative vorticity. Clearly, there are several reasons why no perfect agreement can be expected. First, previous studies were undertaken for other time periods and used different datasets with mostly coarser spatial resolution. Second, some of them looked at different fields or filtered SLP fields to identify cyclones. And third, there are significant differences in the methodologies. The present cyclone frequency fields, f_c , contain cyclones without constraints about their minimum lifetime. Therefore, a hypothetical thermal low that grows and decays daily leads to a prominent maximum in our f_c field, but is absent in other climatologies that applied cyclone lifetime thresholds of 1–3 days. Also, previous climatologies gave equal weight to small and large cyclones, whereas the present one gives more weight to large cyclones. Nevertheless, despite these differences related to data and methods, it is useful to qualitatively identify consistent (and therefore robust) features between the climatologies and some notable differences that point to their more sensitive characteristics.

First a comparison is made of f_c during DJF in the Northern Hemisphere (Fig. 4a) with the cyclone frequencies of Petterssen (1956), which are based upon observational data from 1899 to 1939. There is good agreement for the two maxima in the Mediterranean, and the ones in the Gulf of Alaska, near the southern tip of Greenland, north of Scandinavia, and over Ethiopia. The major disagreement occurs in areas with high topography (e.g., Sierra Nevada and Alberta ranges, northern India) where the Petterssen climatology has relatively large values. During JJA there is some disagreement over Africa and the Middle East, whereas maxima in the Gulf of California, near the Aleutian Islands, in the band between Newfoundland and Iceland, in the Amur valley (50°N , 125°E) and in the Gulf of Tonkin (20°N , 105°E), for instance, are represented in both climatologies.

Considering cyclogenesis, there is a remarkable and

detailed agreement between our Fig. 6a and the winter results by Petterssen (1956). Some differences occur over the Asian continent, near Greenland, where the Petterssen climatology has the maximum on the western side of Greenland and ours on the eastern side; and near Japan, where in the Petterssen study genesis occurs frequently as far south as 25°N. Also for the summer season, the agreement is quite good. Several regions with frequent genesis in the sub- and extratropics can be found with similar amplitude in both datasets. An exception is the very intense peak of cyclogenesis over Spain in the Petterssen climatology, which might be due to short-lived thermal lows that are excluded by the 24-h minimum lifetime criterion that we applied when determining cyclone genesis and lysis.

Comparison with the results from Whittaker and Horn (1984, hereafter WH84) who used synoptic weather charts for the period 1958–77, reveals excellent agreement for several details of the f_c field in midlatitudes (WH84 did not consider subtropical regions). These details include for instance the location of the maximum in the Mediterranean (autumn till spring), the increase from winter to spring over Siberia, the spring maximum in the lee of the northern Ural, the summer maxima over the Hudson Bay/Labrador area and near the Aleutian Islands, and in autumn the local maxima in the eastern Pacific and west of Kamchatka. The largest difference occurs in winter, where the Atlantic maximum is further southwest in the analysis by WH84. This shift might be influenced by the different counting method, since WH84 consider stationary cyclones in the same grid box only once. For cyclogenesis, the present study agrees less with the results by WH84 than with the results by Petterssen discussed above. For the peak areas of cyclogenesis there is reasonable correspondence but genesis according to WH84 occurs only in well-defined areas whereas our climatology indicates a broader geographical distribution.

During winter, our f_c field can be compared with the SLP feature density field of HH02, who studied ERA-15 reanalyses and operational analyses for the period 1979–93. There is relatively good agreement between the two fields, keeping in mind that the f_c field has a smoother structure because it considers cyclones not as points but as finite features. The largest differences occur over eastern Asia where the feature density of HH02 is more prominent than the relatively low values of $f_c < 5\%$. A comparison of the distributions of genesis and lysis with HH02 can be undertaken by considering their Figs. 5c, d and a recomputation of our genesis and lysis fields when applying also a lifetime threshold of 2 days (not shown). The results are similar, but in the HH02 climatology cyclogenesis over land (central

North America, eastern Asia) is much more frequent than in our study, while genesis for instance in the Sea of Japan is weaker. It is not clear whether these discrepancies are due to the differences in the datasets, the tracking algorithm or the spatial filtering applied by HH02. It is also interesting to qualitatively compare the genesis density for lysis in the Gulf of Alaska (HH02; Fig. 7b) with our corresponding relative cyclone frequency field (Fig. 9c). It seems that there are less long-distance tracks from the western Pacific in the HH02 analysis. This might be because the removal of the planetary scales that have a SLP minimum in the central Pacific (HH02; Fig. 2c).

There is close correspondence of the location of the maxima in the wintertime cyclone frequency field shown in Fig. 4a and the one shown by Paciorek et al. (2002), which is also based on a nontracking approach. Comparison between Fig. 6a and the climatology of cyclogenesis produced by Sickmüller et al. (2000), who studied ERA-15 reanalyses and operational analyses for the period 1979–97, is difficult since they only considered cyclones that exist for at least 3 days. Recomputation of the wintertime climatology of genesis for the same category of cyclones (not shown) leads to a reasonable agreement, except for the eastward shift of about 1000 km of the peaks in the western North Atlantic and in the Gulf of Genoa in the study by Sickmüller et al. (2000). The National Centers for Environmental Prediction (NCEP) reanalysis system densities presented by Simmonds and Keay (2002) for the winter season are also not unlike the distribution shown in Fig. 4a, except for a strong peak in the Sea of Okhotsk in their climatology. During summer (Fig. 4c), the qualitative agreement is even better, in particular for the midlatitude maxima east of the Hudson Bay, south of Iceland, and near the Aleutian Islands. Another comparison can be made for wintertime cyclogenesis (Figs. 6a and 7a) with the study of Sinclair (1997), based upon twice-daily ECMWF analyses. The agreement is relatively good in the Northern Hemisphere (except for a more pronounced concentration of genesis in the western parts of the Atlantic and Pacific in the analysis by Sinclair), but less so in the Southern Hemisphere. Again this might be due to differences in cyclone identification, minimum cyclone lifetimes, and data resolution.

In the SH, the long-term climatology by Simmonds and Keay (2000b, hereafter SK00) based on NCEP reanalyses for almost the same time period, reveals a very good agreement, with the exception of the large system density maxima in the Weddell (76°S, 45°W) and the Ross Seas (80°S, 150°W) in SK00. Several details of the SK00 system density field can be found in f_c (Fig. 5).

Examples are the subtropical maxima over Australia and west of Madagascar in DJF and the split in the Tasman Sea/New Zealand region in JJA with low values between 45° and 55°S. Also for genesis and lysis there is close correspondence between the two climatologies. This good agreement (except for the Weddell and Ross Seas) is confirmed by the more recent study by Simmonds et al. (2003) who focused on the synoptic activity near Antarctica.

Finally it is noted that the results presented in this study also agree well with several detailed local cyclone climatologies. This comparison is not meant to be complete and only a few studies are mentioned briefly. For example, the major regions of cyclogenesis in the western North Pacific in our results (Fig. 6) correspond closely to the analyses by Yoshida and Asuma (2004). Further west, in the lee of Altai-Sayan and near Lake Baikal, there is good agreement with the study by Chen et al. (1991). Over North Africa during spring (Fig. 4b) the enhanced cyclone frequencies correspond to the occurrence of Sharav cyclones (Alpert and Ziv 1989). The high values of both genesis and lysis near the southern tip of Greenland have also been discussed by Serreze et al. (1997). Also in agreement with our Fig. 10b they concluded that half of the Icelandic cyclones originate relatively far north, but some can be traced back to the central United States. For the Mediterranean, a comparison can be made with the results by Trigo et al. (1999). Here, the only major difference is the absence of cyclogenesis in the eastern Mediterranean during summer in our study. The cyclones in northern Argentina (Fig. 5), which are frequent in all seasons, have been studied by Seluchi et al. (2003) who identified different dynamical mechanisms for these systems in winter and summer.

To summarize, this very qualitative comparison indicates that our results in general agree well with previous manually and computer-generated climatologies. Significant differences occur however near and over the continents, in particular near high mountains. A more quantitative comparison of the methods would be highly desirable but is presently not possible due to the differences in the time periods, datasets, and variables considered in the different studies.

7. Summary and further remarks

This study introduced a technique that allows the compilation of climatological frequency distributions of local extrema of meteorological fields, considering the features' spatial extent. In the first part of the study, it has been applied to the sea level pressure field from the ERA-40 dataset and a global climatology of cyclones

has been produced for the time period 1958–2001. In principle, the same technique could also be applied to different variables like geopotential height or relative vorticity, to filtered fields (cf. Anderson et al. 2003), or to anomaly fields, where a suitable long-term mean was subtracted previously from the full field.

The resulting climatological cyclone frequency distribution possesses distinct maxima in the well-known areas of intense baroclinic wave activity and in general compares well with previous manual or automated global and regional cyclone climatologies. The main advantages of the new climatology are (i) the consideration of cyclone size (given by the region bounded by the outermost closed SLP contour) as a proxy for their area of influence, and (ii) the straightforward interpretation of the frequency field, that corresponds at any location to the probability of this point being located within a cyclone.

In the second part of the study, a conventional tracking algorithm has been applied to gain additional information about the identified cyclones, in particular their locations of genesis and lysis. In combination with the cyclone identification technique it was then possible to extract subsets of the total cyclone frequency field for specific regions of cyclone origin, passage, or decay. Such a quantitative analysis reveals important detailed information about the behavior of extratropical cyclones. For example, it has been shown that in about 2%–3% of the wintertime instants a cyclone is located over Ireland/Scotland that originated in the western North Atlantic along the U.S. east coast. This type of cyclones corresponds to only 10%–20% of all cyclones in the U.K. region, indicating that a major part of cyclones in this area are generated further east, in the central North Atlantic.

As this is a global cyclone climatology, it is interesting to briefly point out some interhemispheric differences. When doing so, it should however be kept in mind that the ERA-40 dataset has not a uniform quality and is likely to be less reliable in the SH (Bengtsson et al. 2004). In the NH the maxima of cyclone frequencies are in the latitude belts 35°–60°N (Pacific) and 40°–70°N (Atlantic), whereas in the SH this belt is much closer to the pole (55°–70°S). The seasonal cycle is very pronounced in almost all NH regions, but it is rather small in the maximum frequency band encircling Antarctica. As for the cyclone frequency there is a latitudinal shift between the two hemispheres in the main regions of wintertime cyclogenesis: in the NH genesis is largest near 40°N, in the SH cyclones also originate near 40°S but more frequently at higher latitudes (60°–70°S). Cyclolysis peaks poleward of about 55°N/S in both hemispheres. The evaluation of cyclones for spe-

cific regions of genesis, passage or lysis was not systematic (because some regions of interest were chosen subjectively) but nevertheless indicated that some SH tracks extend zonally over more than 180° , a distance that has not been reached by NH cyclones.

In the future, further aspects of this ERA-40 cyclone frequency dataset could be explored and, in addition, the method and the cyclone dataset may be utilized to investigate different aspects of extratropical weather systems and the link between them. The list of possibilities includes:

- The interannual variability of the cyclone frequency field and its link to the principal modes of atmospheric variability and to blocking will be looked at in a follow-up study.
- Special categories of cyclones could be analyzed, like moving and stationary (Nielsen and Dole 1992; Sinclair 1995), deep (Schinke 1993), and explosively deepening (Sanders and Gyakum 1980; Lim and Simmonds 2002) cyclones.
- The present climatology could be complemented by an analysis of SLP maxima to obtain climatological frequency fields of near-surface anticyclones.
- The cyclone frequency field can be compared qualitatively with climatologies of other atmospheric phenomena [cf. the comparison with stratosphere–troposphere exchange events by Sprenger and Wernli (2003)]. Alternatively, the individual identified cyclones (cf. Fig. 2) can be used for a detailed one to one comparison with other meteorological features [like the investigation of the link between cyclones and warm conveyor belts by Eckhardt et al. (2004)]. Studies of this kind can provide novel and quantitative insight into the role of midlatitude cyclones for different aspects of the atmospheric flow system.
- The cyclone identification technique can be used to validate extratropical cyclones in general circulation models and to intercompare different model versions and scenarios, as well as to assess the accuracy of cyclone forecasts and to compare different analysis systems in a feature-based way, as done previously by Hodges et al. (2003).

This brief outlook indicates that the technique introduced in this study and its application to the ERA-40 dataset offer interesting results and exciting possibilities for future research on extratropical cyclones and anticyclones.

Acknowledgments. We are grateful to MeteoSwiss and the ECMWF for providing access to the reanalysis data. HW would like to thank Huw Davies for suggesting (several years ago) the use of the contour searching

algorithm for the identification of cyclones. CS acknowledges funding through the Swiss NCCR climate program. We also thank Ian Simmonds and an anonymous reviewer for their insightful comments.

APPENDIX

Some Details about the Contour Searching Technique

The methodology outlined in section 2a [step (ii)] is strongly based on the accurate identification of SLP contours. For instance, if a local SLP minimum is identified with $p(\mathbf{x}_1) = 991.5$ hPa then the contour with the pressure value $p(C_{1,1}) = p(\mathbf{x}_1) + \Delta p = 993.5$ hPa needs to be identified as a polygon of points $C_{1,1}(n)$, all with a SLP value of 993.5 hPa. If the contour $C_{1,1}$ is closed, then starting from \mathbf{x}_1 in any direction will lead to a point on the contour. At that point the local gradient of the SLP field is determined and rotated by 90° to obtain the tangent vector along the contour $C_{1,1}$. As a first guess for the next point of the contour, a step is performed along this direction with a subjectively chosen length of 0.3° . It should be a reasonable assumption to use a step distance that is about half of the SLP field's horizontal resolution. Usually this first guess point is not exactly on the contour and a small step along the local SLP gradient at the first guess point is required to find the second point of the contour's polygon. From there the same procedure is applied to find the third point, etc., until a newly found contour point $C_{1,1}(N)$ is closer to the first contour point $C_{1,1}(1)$ than to the previous one $C_{1,1}(N - 1)$. At that stage the entire (closed) contour is found and the search can begin for the next contour with the SLP value $p(C_{1,2}) = p(\mathbf{x}_1) + 2\Delta p$.

REFERENCES

- Alpert, P., and B. Ziv, 1989: The Sharav cyclone: Observations and some theoretical considerations. *J. Geophys. Res.*, **94**, 18 495–18 514.
- Anderson, D., K. I. Hodges, and B. J. Hoskins, 2003: Sensitivity of feature-based analysis methods of storm tracks to the form of background field removal. *Mon. Wea. Rev.*, **131**, 565–573.
- Bengtsson, L., K. I. Hodges, and S. Hagemann, 2004: Sensitivity of the ERA-40 reanalysis to the observing system: Determination of the global atmospheric circulation from reduced observations. *Tellus*, **56A**, 456–471.
- Blackmon, W. L., J. M. Wallace, N.-C. Lau, and S. L. Mullen, 1977: An observational study of the Northern Hemisphere wintertime circulation. *J. Atmos. Sci.*, **34**, 1040–1053.
- Blender, R., and M. Schubert, 2000: Cyclone tracking in different spatial and temporal resolutions. *Mon. Wea. Rev.*, **128**, 377–384.
- , K. Fraedrich, and F. Lunkeit, 1997: Identification of cyclone-track regimes in the North Atlantic. *Quart. J. Roy. Meteor. Soc.*, **123**, 727–741.

- Chen, S.-J., Y.-H. Kuo, P.-Z. Zhang, and Q.-F. Bai, 1991: Synoptic climatology of cyclogenesis over East Asia, 1958–1987. *Mon. Wea. Rev.*, **119**, 1407–1418.
- Eckhardt, S., A. Stohl, H. Wernli, P. James, C. Forster, and N. Spichtinger, 2004: A 15-year climatology of warm conveyor belts. *J. Climate*, **17**, 218–237.
- Emanuel, K., 2003: Tropical cyclones. *Annu. Rev. Earth Planet. Sci.*, **31**, 75–104.
- Fyfe, J. C., 2003: Extratropical Southern Hemisphere cyclones: Harbingers of climate change? *J. Climate*, **16**, 2802–2805.
- Grotjahn, R., D. Hodys, and C. Castello, 1999: Do frontal cyclones change size? Observed widths of North Pacific lows. *Mon. Wea. Rev.*, **127**, 1089–1095.
- Haak, U., and U. Ulbrich, 1996: Verification of an objective cyclone climatology for the North Atlantic. *Meteor. Z.*, **5**, 24–30.
- Hall, N. M. J., B. J. Hoskins, P. J. Valdes, and C. A. Senior, 1994: Storm tracks in a high-resolution GCM with doubled carbon dioxide. *Quart. J. Roy. Meteor. Soc.*, **120**, 1209–1230.
- Hanson, C. E., J. P. Palutikof, and T. D. Davies, 2004: Objective cyclone climatologies of the North Atlantic—A comparison between ECMWF and NCEP reanalyses. *Climate Dyn.*, **22**, 757–769.
- Hodges, K. I., B. J. Hoskins, J. Boyle, and C. Thorncroft, 2003: A comparison of recent reanalysis datasets using objective feature tracking: Storm tracks and tropical easterly waves. *Mon. Wea. Rev.*, **131**, 2012–2037.
- Hoskins, B. J., and K. I. Hodges, 2002: New perspectives on the Northern Hemisphere winter storm tracks. *J. Atmos. Sci.*, **59**, 1041–1061.
- Köppen, W., 1881: Die Zugstrassen der barometrischen Minima in Europa und auf dem nordatlantischen Ocean und ihr Einfluss auf Wind und Wetter bei uns. *Mitt. Geograph. Ges. Hamburg*, **1**, 76–97.
- Kurz, M., 2004: On the dynamics of the splitting process of cyclones near southern Greenland. *Meteor. Z.*, **13**, 143–148.
- Lambert, S. J., 1988: A cyclone climatology of the Canadian Climate Centre general circulation model. *J. Climate*, **1**, 109–115.
- Lim, E.-P., and I. Simmonds, 2002: Explosive cyclone development in the Southern Hemisphere and a comparison with Northern Hemisphere events. *Mon. Wea. Rev.*, **130**, 2188–2209.
- McCabe, G. J., M. P. Clark, and M. C. Serreze, 2001: Trends in Northern Hemisphere surface cyclone frequency and intensity. *J. Climate*, **14**, 2763–2768.
- Nielsen, J. W., and R. M. Dole, 1992: A survey of extratropical cyclone characteristics during GALE. *Mon. Wea. Rev.*, **120**, 1156–1167.
- Paciorek, C. J., J. S. Risbey, V. Ventura, and R. D. Rosen, 2002: Multiple indices of Northern Hemisphere cyclone activity, winters 1949–99. *J. Climate*, **15**, 1573–1590.
- Petterssen, S., 1956: *Weather Analysis and Forecasting*. Vol. 1. 2d ed. McGraw-Hill, 428 pp.
- Raible, C. C., and R. Blender, 2004: Northern Hemisphere mid-latitude cyclone variability in GCM simulations with different ocean representations. *Climate Dyn.*, **22**, 239–248.
- Robertson, F. R., and P. J. Smith, 1980: The kinetic energy budgets of two severe storm producing extratropical cyclones. *Mon. Wea. Rev.*, **108**, 127–143.
- Sanders, F., and J. R. Gyakum, 1980: Synoptic-dynamic climatology of the “bomb.” *Mon. Wea. Rev.*, **108**, 1589–1606.
- Schinke, H., 1993: On the occurrence of deep cyclones over Europe and the North Atlantic in the period 1930–1991. *Contrib. Atmos. Phys.*, **66**, 223–237.
- Schwierz, C. B., and H. C. Davies, 2003: Evolution of a synoptic-scale vortex advecting toward a high mountain. *Tellus*, **55A**, 158–172.
- Seluchi, M. E., A. C. Saulo, M. Nicolini, and P. Satyamurty, 2003: The northwestern Argentinean low: A study of two typical events. *Mon. Wea. Rev.*, **131**, 2361–2378.
- Serreze, M. C., F. Carse, R. G. Barry, and J. C. Rogers, 1997: Icelandic low cyclone activity: Climatological features, linkages with the NAO, and relationships with recent changes in the Northern Hemisphere circulation. *J. Climate*, **10**, 453–464.
- Sickmüller, M., R. Blender, and K. Fraedrich, 2000: Observed winter cyclone tracks in the Northern Hemisphere in re-analysed ECMWF data. *Quart. J. Roy. Meteor. Soc.*, **126**, 591–620.
- Simmonds, I., 2000: Size changes over the life of sea level cyclones in the NCEP reanalyses. *Mon. Wea. Rev.*, **128**, 4118–4125.
- , and K. Keay, 2000a: Variability of Southern Hemisphere extratropical cyclone behavior, 1958–97. *J. Climate*, **13**, 550–561.
- , and —, 2000b: Mean Southern Hemisphere extratropical cyclone behavior in the 40-year NCEP–NCAR reanalysis. *J. Climate*, **13**, 873–885.
- , and —, 2002: Surface fluxes of momentum and mechanical energy over the North Pacific and North Atlantic Oceans. *Meteor. Atmos. Phys.*, **80**, 1–18.
- , —, and E.-P. Lim, 2003: Synoptic activity in the seas around Antarctica. *Mon. Wea. Rev.*, **131**, 272–288.
- Simmonds, A. J., and J. K. Gibson, 2000: The ERA-40 project plan. ERA-40 Project Report Series 1, ECMWF, Reading, United Kingdom, 63 pp.
- Sinclair, M. R., 1995: A climatology of cyclogenesis for the Southern Hemisphere. *Mon. Wea. Rev.*, **123**, 1601–1619.
- , 1997: Objective identification of cyclones and their circulation intensity, and climatology. *Wea. Forecasting*, **12**, 595–612.
- , and G. Watterson, 1999: Objective assessment of extratropical weather systems in simulated climates. *J. Climate*, **12**, 3467–3485.
- Sprenger, M., and H. Wernli, 2003: A northern hemispheric climatology of cross-tropopause exchange for the ERA15 time period (1979–1993). *J. Geophys. Res.*, **108**, 8521, doi:10.1029/2002JD002636.
- Trigo, I. F., T. D. Davies, and G. R. Bigg, 1999: Objective climatology of cyclones in the Mediterranean region. *J. Climate*, **12**, 1685–1696.
- Whittaker, L. M., and L. H. Horn, 1984: Northern Hemisphere extratropical cyclone activity for four mid-season months. *J. Climatol.*, **4**, 297–310.
- Yoshida, A., and Y. Asuma, 2004: Structures and environment of explosively developing extratropical cyclones in the Northwestern Pacific region. *Mon. Wea. Rev.*, **132**, 1121–1142.
- Zhang, X., J. E. Walsh, J. Zhang, U. S. Bhatt, and M. Ikeda, 2004: Climatology and interannual variability of Arctic cyclone activity: 1948–2002. *J. Climate*, **17**, 2300–2317.
- Zolina, O., and S. K. Gulev, 2002: Improving the accuracy of mapping cyclone numbers and frequencies. *Mon. Wea. Rev.*, **130**, 748–759.